FUNCTIONALIZATION OF SWNTS WITH COUMARIN-LABELED POLYMERS

FUNCTIONALIZATION OF SINGLE-WALLED CARBON NANOTUBES WITH COUMARIN-LABELED POLYMERS

By

HAI WANG, B.Sc.

A Thesis

Submitted to the School of Graduate Studies

in Partial Fulfillment of the Requirements

for the Degree

Master of Science

McMaster University

MASTER OF SCIENCE (2004) McMaster University

(Chemistry) Hamilton, Ontario

TITLE: Functionalization of Single-Walled Carbon Nanotubes with Coumarin-labeled Polymers

AUTHOR: Hai Wang, B.Sc.

SUPERVISOR: Professor Alex Adronov

NUMBER OF PAGES: xiv, 99

Abstract

Single-walled carbon nanotubes (SWNTs) are a new class of materials that have recently attracted a great deal of interest because of their unique structural, mechanical, and electronic properties. Also, SWNTs have a high potential for a number of technological applications, including molecular electronics, emissive devices, and photovoltaic devices. To fully utilize their unique properties, control of the solubility, processibility, and functionality of SWNTs is required. Therefore chemical functionalization of SWNTs using a variety of methods, in either covalent or noncovalent manner, has been developed to produce soluble nanotube composites coupled with various chemical moieties. To explore the possibility of making potential soluble nanotube-based materials for solar cells, SWNTs were functionalized with organic chromophore-labeled polymers via a radical coupling process. The organic chromophore was used to absorb light to produce photo-induced electrons, while the polymer chains were used for improving the solubility of SWNTs. These novel chromophore-labeled polymers were made by stable free radical polymerization (SFRP), either using a synthetic chromophore-functionalized styrenic monomer or by derivatizing well-defined polystyrenes. Specifically, the chromophores employed in this investigation were

commercially available 7-hydroxycoumarin and coumarin-343. In order to carry out fluorescence studies of SWNT-coumarin composites systematically, various factors were probed by (1) altering polystyrene lengths between the SWNT and the coumarin; (2) changing the distribution of coumarins along the polymer chain, in the form of either a block or random copolymer; (3) placing single coumarins on the surface of SWNTs. All of these resulting polymer functionalized SWNTs were found to be soluble in certain organic solvents such as $CHCl_3$. Different absorption behaviors have been observed for SWNTs functionalized with 7-hydroxycoumarin containing copolymers. Fluorescence was still observable for all of these composites, and the π-π interactions between coumarins and nanotubes were believed to be responsible for the broadening of emission bands of the resulting composites.

Acknowledgements

I would like to extend my sincere gratitude and appreciation to my supervisor, Dr. Alex Adronov, for his tireless guidance, patience, and encouragement. I am extremely thankful to him for giving me the opportunity to be part of the group – I have learned a wealth of knowledge inside and outside of chemistry for the past two years.

.

To the members of our group: Yuanqin Liu – thank you for your discussion and suggestions along the way, and help for TEM; Matthew Parrott, Greg Bahun – the beers, golf outings, and conversations we had made my stay at Mac memorable; Stephanie Gratton, Rahima Benhabbour – the lab was a more comfortable place with your smiles; Zhaoling Yao, Clair Wang – the start of my life in Canada would have been harder without your help; Jim Mayo – thank you for your input in the lab.

I would also like to thank Dr. Stover's group for the use of their equipment and discussions on chemistry.

My thanks also go to Andy Duft, Dr. Donald Hughes, and George Timmins for helping me with my experiments.

I owe a debt of gratitude to my family for their guidance and unwavering support throughout my life. They were behind me at every point in my life, even when I did not really know where I was going. I can only hope to show the same kind of dedication and love to them.

A final acknowledgement goes to my beloved Rui Gu for being so understanding and patient when I was working late nights and weekends, and giving me the motivation to succeed in finishing my degree.

Table of Contents

List of Schemes

List of Figures

Chapter 1 Introduction

1.1 Single-Walled Carbon Nanotubes (SWNTs) - Structure, Properties, and Potential Applications

As the fourth allotrope of carbon, Multi-Walled Carbon Nanotubes (MWNTs) were first discovered by Ijima in 1991.[1] Two years later, the other category of carbon nanotubes called Single-Walled Carbon Nanotubes (SWNTs) were also found by Ijima and coworkers.[2] SWNTs have one shell of carbon atoms, while MWNTs consist of multiple, nested carbon tubes. Although both MWNTs and SWNTs are composed entirely of sp^2 hybridized carbon atoms, SWNTs are relatively much more uniform and defect free structures in comparison to MWNTs.[3] SWNTs can be thought of as a single graphene sheet and rolled up into a hollow seamless cylinder (Figure 1).

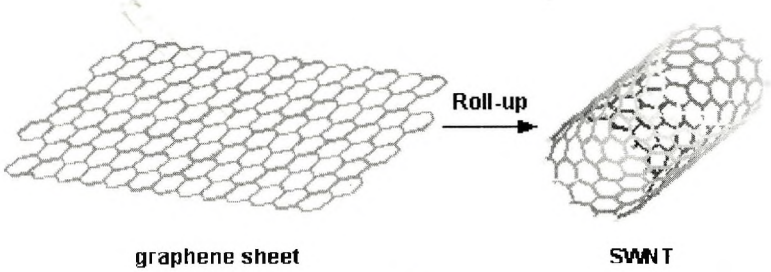

Figure 1. Schematic representation of a graphene sheet and a single-walled carbon nanotube.

With diameters typically between 0.7 and 2 nm, the well-defined cylindrical structures vary from microns to multiple centimeters in length, which provides them with a high aspect ratio.[4,5] The ends may be open or capped with the equivalent of half a fullerene molecule. Since the rolling up can be done in many ways, the structure of a SWNT is therefore determined not only by its diameter, but also by the pitch angle of the helix. The commonly applied notation for the structure is in the form of a pair of integers m and n, which measure the pitch and the circumference, respectively, of the nanotube in lattice units (Figure 2)[6], and are called lattice translational indices of the graphene plane. This is a very important scheme in characterizing the properties of individual nanotubes since it presents the essential symmetry to the nanotube structure.[7] For instance, the diameter can be related to the lattice vectors by the equation $d = 0.078 \times (m^2 + n^2 + mn)^{1/2}$ nm, where d is the diameter of a SWNT. In addition, the chirality (R) of SWNTs is defined by the equation $R = m \times a_1 + n \times a_2$, where a_1 and a_2 are unit vectors of the hexagonal honeycomb lattice. The chiral angle θ is formed between R and the zigzag line. If R lies along the zigzag line (θ=0°), then it is called a "zigzag" nanotube. If θ=30°, then the tube is of the "armchair" type. If $0° < \theta < 30°$, then it is a "chiral" tube (Figure 3).[8,9]

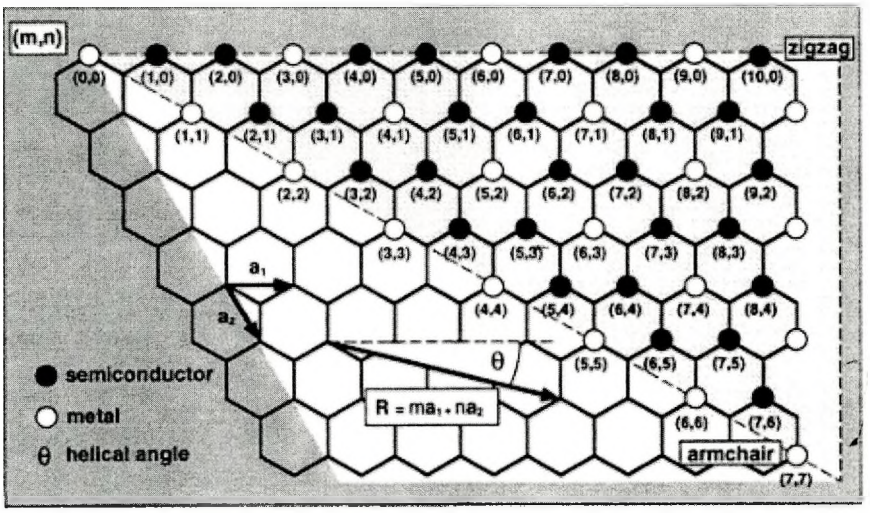

Figure 2. Indexing scheme that shows the folding procedure to create nanotube cylinders from planar graphene sheets. $\mathbf{a}_1$ and $\mathbf{a}_2$ are the primitive lattice vectors of the hexagonal lattice. The position and length of the vector, **R**, connecting an origin to the lattice point that defines the nanotube index, determine the helicity and diameter of the tube. All the (*n*, *n*) type nanotubes form armchair tubes and all (*n*, 0) tubes are zigzag tubes. (Reprinted from ref. 6)

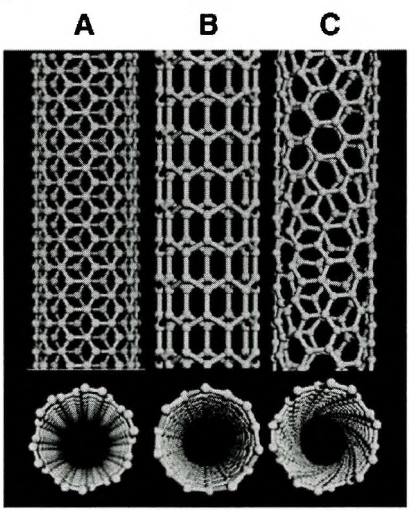

Figure 3. Schematic illustrations of the structures of (A) armchair, (B) zigzag, and (C) chiral SWNTs. Projections normal to the tube axis and perspective views along the tube axis are on the top and bottom, respectively. (Reprinted from ref. 9)

The values of *m* and *n* determine the chirality of the nanotube. The chirality in turn affects its lattice structure, and other properties such as density and conductance. Due to the strong van der Waals interactions (π-π stacking) that exist between the surfaces of the tubes, carbon nanotubes tend to pack parallel to one other, forming intertwined bundles or ropes composed of both metallic and semiconducting tubes.[10]

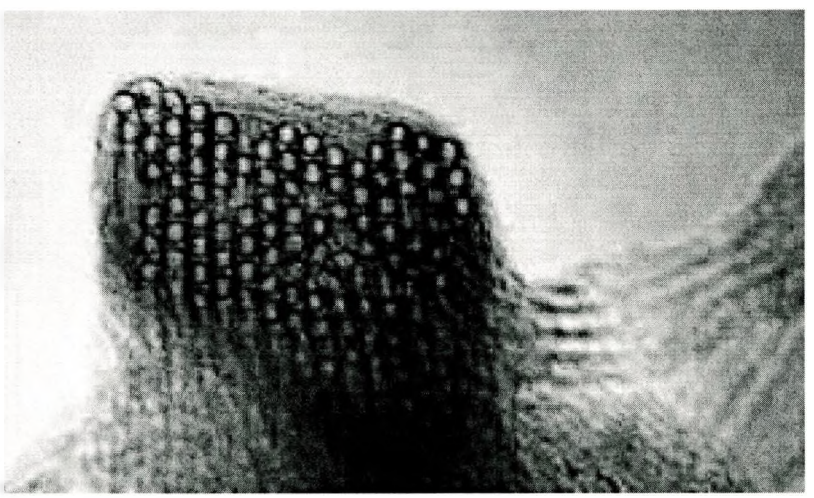

Figure 4. TEM cross-section of a single nanotube rope made of about 100 SWNTs with uniform diameters (1.4 nm). The SWNTs pack in a triangular lattice. (Reprinted from ref. 10)

Theory predicts that the electronic structure of SWNTs depends critically on these chiral indices. In particular, if | *m*–*n* | is a multiple of three, then the nanotube is a one-dimensional metal because, in these cases, the density of electronic states at the Fermi level is non-zero. Therefore, one third of the SWNTs in a given batch are expected to be metallic, and the remaining two thirds are

semiconducting. [8,11,12] In addition to their conductivity properties, the mechanical strength (Young's modulus) of SWNTs lies close to 1 Tpa, which is five times stronger than steel. [13,14] It has also been reported recently that they exhibit thermal conductivity as high as diamond [15] and high mechanical resilience,[16,17] which allows them to be bent without breaking.

Due to their high tensile strength and high mechanical resilience, incorporation of SWNTs into plastics can potentially provide structural materials with significantly increased modulus and strength. Some promising results have been reported.[18,19] For instance, for epoxy, Biercuk and co-workers observed a monotonic increase of resistance to indentation (Vickers hardness) by 3.5 times with a 2% SWNTs loading and a doubled thermal conductivity with 1% SWNTs.[18] The unique electronic properties of nanotubes make them qualified for use as quantum wires and in heterojuction devices. Based on a single semiconducting SWNT the Delft group has built the first single-molecule field-effect transistor, an essential component for next-generation computing.[20] Field emission devices are one of the more promising nanotube applications being developed by industry and academia, which utilize SWNTs as field emission electron sources.[21,22] It is also suggested that SWNTs could possibly be used as miniature chemical or biological sensors since their conductivity can differ by 2 to

3 orders of magnitude when they are exposed to certain types of gases in ppm level, such as ammonia (NH_3),[23] nitrous oxide (NO_2),[23] and oxygen (O_2).[24] The mechanical robustness of SWNTs and the low buckling force together with their conductivity make it possible to use SWNTs as Atomic Force Microscopy (AFM) tips,[25,26] which are now commercially available from Daiken Chemical Company, Ltd. Other applications of SWNTs include electrochemical devices that make use of the high electrochemically accessible surface area of porous nanotube arrays combined with their high electronic conductivity[27-29] as well as hydrogen storage for fuel cells that may, one day, power electric vehicles or laptop computers[30-33].

SWNTs have also been utilized in photovoltaic devices by Kymakis and co-workers from Cambridge University.[34-36] This group has developed poly(3-octylthiophene) (P3OT) based photovoltaic devices that, when doped with SWNTs, have an increased photocurrent by more than two orders of magnitude and exhibit a doubling of the open-circuit voltage. These nanotube diodes were made by depositing SWNT-containing P3OT films onto glass substrates coated with indium-tin oxide (ITO). Aluminum electrodes were then thermally evaporated under a vacuum to form a sandwich configuration (Figure 5). P3OT acts as the photo-induced electron donor, while SWNTs act as the electron acceptors and also allow the transferred electrons to be transported by providing

percolation paths. It is proposed that the improvement in the photovoltaic properties of the blend device arises from the introduction of internal polymer/nanotube junctions within the polymer matrix. These junctions perform as dissociation centers, which split up the excitons, bind electron–hole pairs caused by the photon absorption of organic materials and also produce a continuous pathway for the electrons to be efficiently transported to the negative electrode. This leads to an increase in the electron mobility, and therefore balances the charge carrier transport to the electrodes resulting in enhanced charge separation and collection.

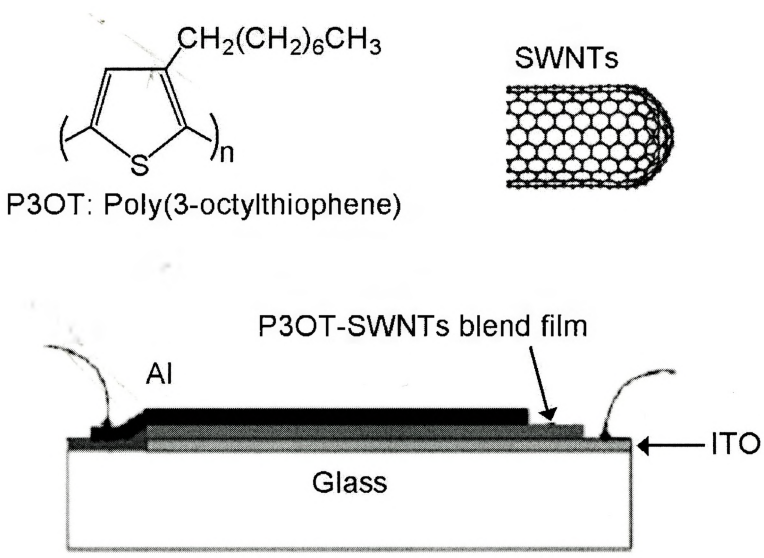

Figure 5. Chemical structures of P3OT, SWNTs and device architecture of the photovoltaic cell.

1.2 Functionalization of SWNTs

SWNTs, despite their useful potential, have not been widely integrated into applications, in part because of the lack of controlled solubility and processibility in solvents. To fully utilize their unique properties, and broaden the scope of their technological applications, it is necessary that not only small molecules, but also large ensembles of SWNTs can be manipulated and studied by analytical methods. Thus chemical functionalization of SWNTs is a particularly appealing goal for chemists and materials scientists, as it can improve solubility and processibility[37], and allows the remarkable properties of SWNTs to be combined with other materials.

1.2.1 Chemical Reactivity of SWNTs

A perfect SWNT does not have functional groups, making it a quasi-1D cylindrical aromatic macromolecule that is chemically inert. However, local strains resulting from curvature-induced pyramidalization and misalignment of the π-orbitals of the carbon atoms make carbon nanotubes more reactive than a flat graphene sheet.[38-40] Conceptually, a pristine SWNT can be divided into two regions: two end caps and the sidewall.[41] The fullerene-like end caps of the SWNTs are quite reactive due to the large strain induced primarily from

pyramidalization.[42] The reactivity of the sidewalls of SWNTs is proportionally lower than that of fullerenes since the typical diameter of a SWNT (0.7 – 2 nm) is larger than that of a fullerene. However, some defects of the six-membered ring carbon structure of the sidewall, such as the inclusion of five- or seven-membered rings in the carbon network are introduced in the initial formation of SWNTs, in addition to other structural imperfections introduced during the shortening and purification of pristine SWNTs by sonication in oxidative acids such as HNO_3.[43-45] Defects are important in chemical functionalization of SWNTs since they can act as anchor groups for further derivatization. It has been shown that nanotubes can tolerate a limited number of defects before they lose their unique electronic and mechanical properties.[46,47] Therefore defects can be regarded as a promising starting point for the covalent functionalization of SWNTs.

Considering the low reactivity, solubility or dispersability, and the strong tendency to form bundles of SWNTs, covalent functionalization of the sidewalls can be successful only if a highly reactive reagent is utilized. Despite these difficulties, several approaches to the functionalization of SWNTs have been developed in recent years using both covalent and noncovalent chemistry. These approaches include covalent functionalization of defects and the sidewalls (Figure 6A & B), noncovalent functionalization, such as exohedral formation of

supramolecular adducts with surfactants or polymers (Figure 6C & D), and endohedral doping (Figure 6E).[48]

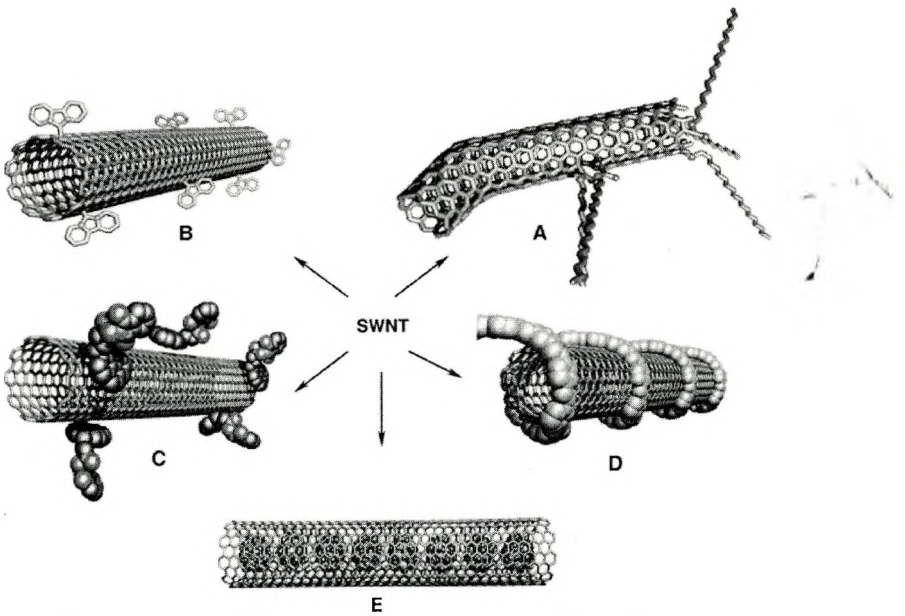

Figure 6. Functionalization possibilities for SWNTs: A) defect-group functionalization, B) covalent sidewall functionalization, C) noncovalent exohedral functionalization with surfactants, D) noncovalent exohedral functionalization with polymers, and E) endohedral functionalization with, for example, C_{60}. For methods B-E, the tubes are drawn in idealized fashion, but defects are found in real situations. (Reprinted from ref. 49)

1.2.2 Covalent Functionalization of SWNTs

Covalent functionalization of SWNTs may be carried out on defect groups as well as sidewalls. As mentioned above, defects are present at the end caps, open ends formed after shortening, and the sidewalls of SWNTs. Under harsh conditions, these defects can be oxidized to carboxylic acid and other weakly acidic functionalities.[43,44,49] These carboxylic acid groups provide handles to

SWNTs that can subsequently be used to couple a variety of molecules mainly by amidation and esterification, to make soluble nanotube materials or novel composites such as nanocrystals[50], biomolecules[51,52] and organometallic complexes[53] (Figure 7).

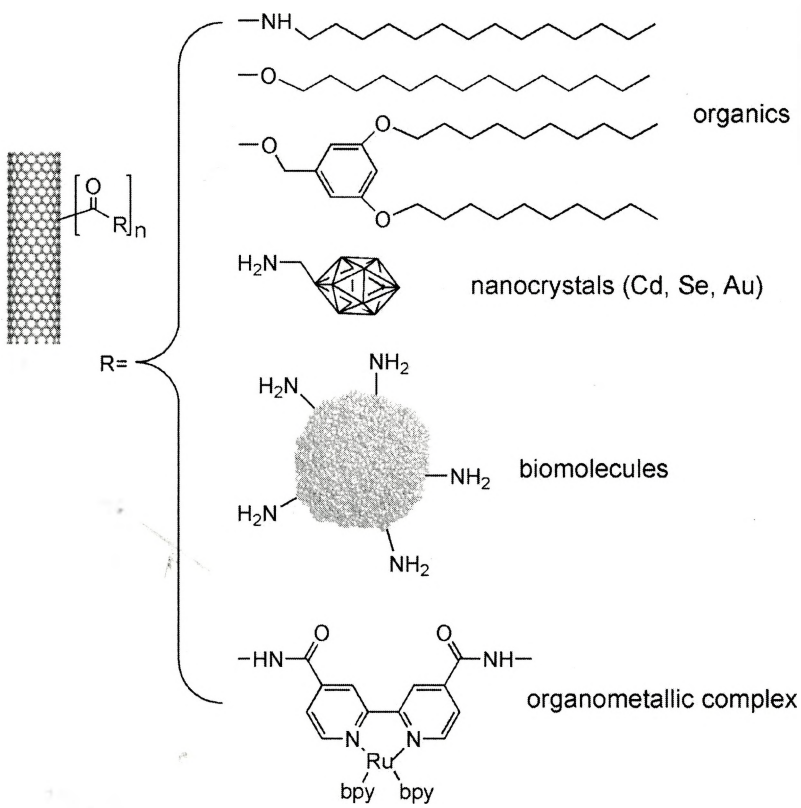

Figure 7. Covalent functionalization of SWNTs via defect groups.

In addition to defect group functionalization, covalent chemistry on the sidewalls of SWNT has also been demonstrated by using a number of chemical processes, including [2+1] cycloaddition of nitrenes,[54,55] hydrogenation via the Birch reduction,[55,56] fluorination,[57,58] alkylation,[59] arylation,[60,61] nucleophilic

carbene addition,[38,54,55] 1,3-dipolar cycloaddition of azomethine ylides,[62] the Bingel reaction (cyclopropanation)[63] and radical addition.[64,65]

In terms of solubility, polymer wrapped SWNTs, which could be made by using above functionalization methods, are among the most soluble samples. It is believed that the long polymer chains help SWNTs dissolve in good solvents even with a low degree of functionalization by breaking the nanotube bundles, which is critical to the solubility. Basically, covalent attachment of polymers to SWNTs can be done either by a "grafting to" approach, in which the polymer is first prepared and then reacted with SWNTs,[66,67] or a "grafting from" approach to the growth of polymers from the surface of nanotubes by first covalently attaching polymerization initiators and then exposing the nanotube-based macroinitiators to monomers.[68,69]

For instance, Yao and coworkers successfully made soluble SWNT-poly(*tert*-butyl acrylate) nanocomposites following a "grafting from" approach.[69] SWNTs were functionalized along the sidewalls with phenol groups using the 1,3-dipolar cycloaddition reaction. These phenol groups were further derivatized with 2-bromoisobutyryl bromide, resulting in the attachment of atom transfer radical polymerization (ATRP) initiators to the sidewalls of the nanotubes, which were active in the polymerization of various monomers, including

tert-butyl acrylate from the surface of the nanotubes. These polymer-functionalized composites were found to be soluble in various organic solvents, and became water-soluble after the *tert*-butyl groups of the polymers were removed.

One challenge that lies in covalent functionalization of carbon nanotubes is that the solubility of the functionalized carbon nanotubes is sometimes strongly dependent on the reaction routes.[70] For example, Sun and coworkers demonstrated that in the amidation with the same amino-containing functional group (Scheme 1), the samples produced from the acyl chloride route were more soluble than those from the diimide-activated coupling reaction.[71-73] The latter normally contain more bundled carbon nanotubes in the soluble fraction indicated by light scattering analysis.

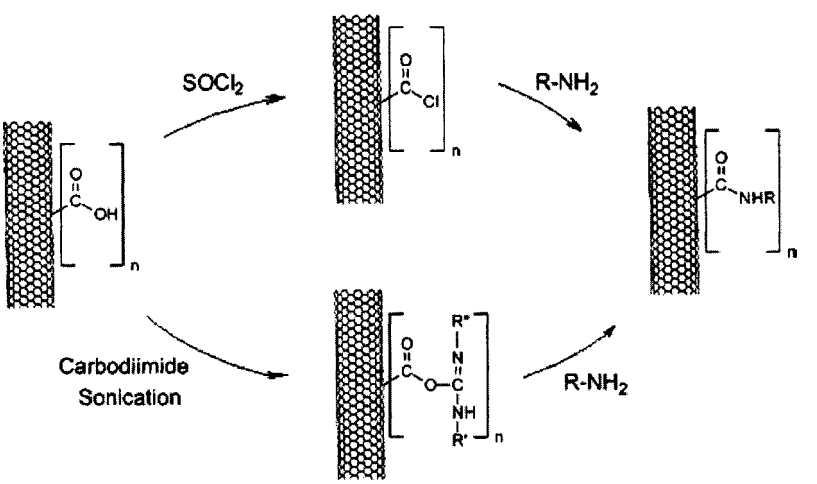

Scheme 1. Two routes to the same functionalization of SWNTs.

1.2.3 Functionalization of Carbon Nanotubes with Radicals

As mentioned above, functionalization of carbon nanotubes with radicals has been reported very recently, using technology developed in the derivatization of fullerenes.[74-76] Attachment of radicals formed in situ from diazonium salts produced functionalized SWNTs.[61] Addition of carbon radicals generated from thermal decomposition of diacyl and dibenzoyl peroxides also led to the formation of functionalized SWNTs.[64] In a similar manner, various functional groups could be added to SWNTs by the introduction of alkyl iodides in the benzoyl peroxide decomposition process.[65] In addition to small molecules, polymers have been also utilized in functionalization of carbon nanotubes via a radical process. Using an in-situ free radical polymerization reaction, Shaffer and Koziol synthesized polystyrene grafted carbon nanotubes, which were soluble in regular organic solvents, including toluene, chloroform and THF.[77] This approach, however, results in poor control over molecular weight and polydispersity in synthesized polymers due to the nature of free radical polymerizations. To prepare carbon nanotubes that are functionalized with polymers with well-defined structures, living free radical polymerizations may be feasible since they work in a controlled manner and, more importantly, radicals can be readily produced during or after polymerization reactions.

1.3 Stable Free Radical Polymerization (SFRP)

Living free radical polymerization (LFRP) is one of the most rapidly developing fields in polymer science and engineering. It offers the opportunity to introduce high degrees of control over physical and chemical properties of polymers through the manipulation of molecular weight, polydispersity, chemical composition and polymer architecture. Improved control over the resultant properties will lead to more efficient polymer production and new polymer products. Ionic polymerization, a well established living polymerization method for making materials with well-defined architecture including controlled molecular weight and narrow polydispersity,[78,79] however, requires a demanding experimental setup and is limited to certain types of monomers. With the ability of providing the control of living polymerizations without the associated demanding experimental conditions, living radical polymerizations have attracted much research interest in polymer science and engineering since the mid 90's. Nitroxide-mediated Stable Free Radical Polymerization (SFRP)[80-83], Atom Transfer Radical Polymerization (ATRP)[84-87], and Reversible Addition Fragmentation Transfer Polymerization (RAFT)[88-91] are three of the most common techniques for living radical polymerizations. They have been widely used for the synthesis of well-defined block, gradient, and alternating copolymers.

In SFRP, Nitroxides such as 2,2,5,5-tetramethyl-3-(1-phenylethoxy)-4-chloromethyl-phenyl-3-azahexane,[83] compound **1**, thermally decompose (Scheme 2) at 125°C to form carbon-centered free radicals (initiating radicals) and oxygen-centered free radicals, 2,2,5,5-tetramethyl-4-phenyl-3-azahexane-3-nitroxide, compound **2** (alkoxyamine derivatives). The oxygen-centered free radicals are essentially stable and will not initiate polymerization, but can couple to existing radicals and act as radical capping agents, thereby decreasing the concentration of free radicals in solution and diminishing termination steps.

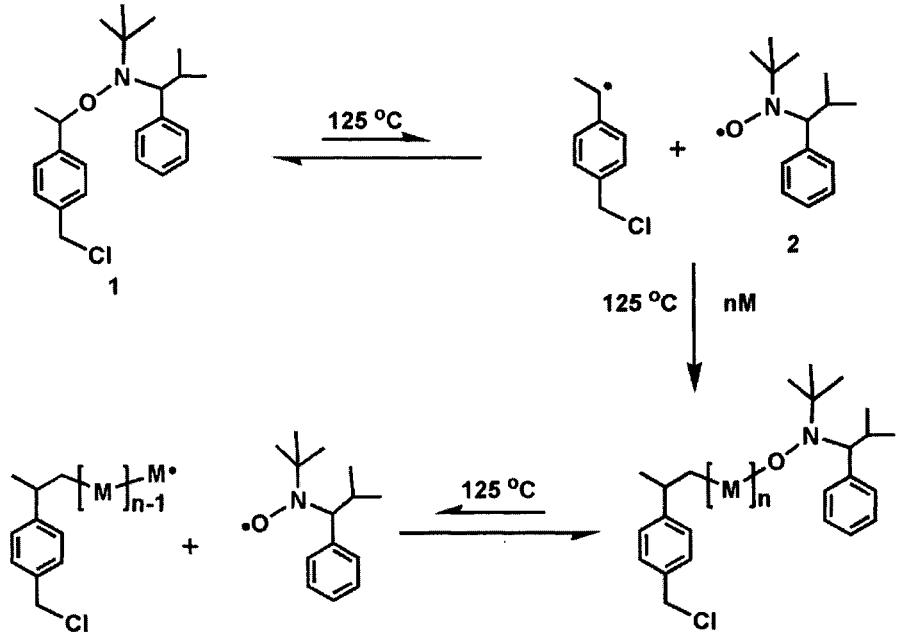

Scheme 2. General mechanism of SFRP using 2,2,5,5-tetramethyl-3-(1-phenylethoxy)-4-chloromethyl-phenyl-3-azahexane as initiator.

Some additives, such as acetic anhydride and stable free nitroxide radicals

(the radical to which the corresponding initiator will thermally decompose) are normally used to obtain a faster polymerization rate and narrower polydispersity, respectively.[92,93] The family of nitroxides[83] permits the polymerization of a wide variety of monomers: acrylates, acrylamides, 1,3-dienes and acrylonitrile. However, to date, styrenics are still the easiest monomer family to be polymerized under SFRP in a living manner.

Chapter 2 Objectives

Our study is targeted toward making soluble SWNT-polymer composites functionalized with organic chromophores, and probing the photo-induced electron transfer behaviors of these composites by studying their fluorescence properties. Covalently functionalized with dye molecules, these SWNTs may lead to a new type of dye-sensitized solar cell material with high efficiency and good processibility given photo-induced electron transfer from chromophores to SWNTs. As mentioned in section 1.2.3, carbon radicals generated by thermal decomposition of diacyl and dibenzoyl peroxides have been shown to couple with the sidewalls of SWNTs, which leads to remarkably improved solubility of SWNTs in organic solvents. Following this idea, it was proposed that SFRP could be utilized to functionalize SWNTs with polymers via the radical coupling reaction at elevated temperature, resulting in SWNTs that exhibit improved solubility. Subsequently, the attached polymers could be used as functional handles to which chromophores can be attached. Nitroxide-terminated polymers bearing a chloromethyl end group made from stable free radical polymerization (SFRP) are appropriate candidates to accomplish this goal since they can produce polymer radicals upon heating to 125 ^{o}C and allow for post-functionalization with chromophores. For successful solubilizations of SWNTs with polymers, the

properties of the polymers (molecular weights and their compositions) are critical. We therefore focused on the functionalization of SWNTs with polystyrene (PS) (scheme 3) and its derivatives with different molecular weights since Ford and Shaffer have shown that PS functionalized carbon nanotube composites are soluble in some organic solvents.[68,77]

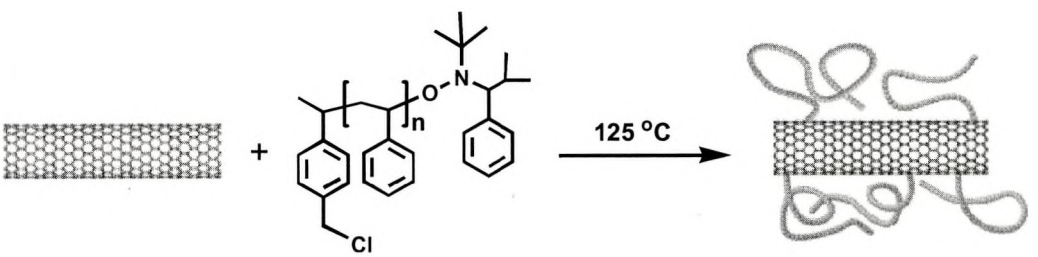

Scheme 3. Functionalization of SWNTs with polystyrene made from SFRP.

Furthermore, the photo-induced electron transfer (PET) behaviors of these SWNT-chromophore composites will depend on not only the distance between electron donor (chromophore) and electron acceptor (SWNT), but also the density and distribution of chromophores along the polymer chains. In order to carry out fluorescence studies of SWNT-chromophore composites systematically, a variety of composite structures were designed, where polymer lengths between the SWNT and the chromophore were varied (Figure 8A-C). Additionally, SWNTs functionalized with chromophore containing block and random copolymers

(Figure 8D & E), as well as SWNTs functionalized with single chromophores on the surface of SWNTs (Figure 8F & G) were envisioned.

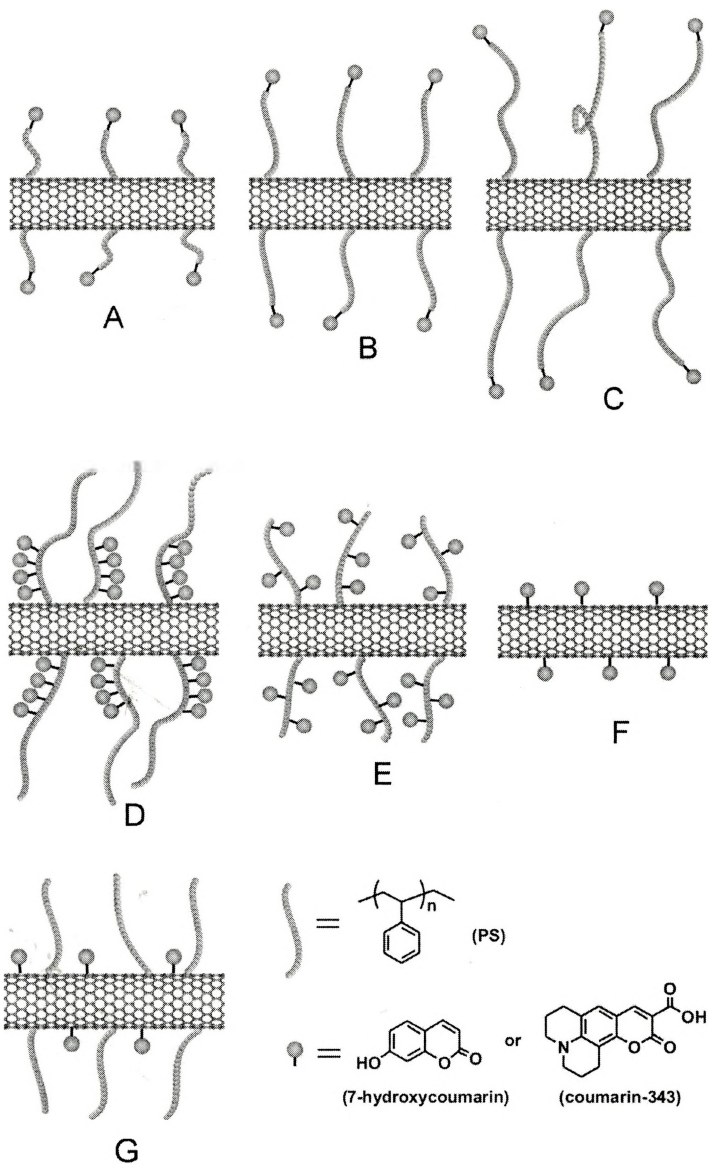

Figure 8. Illustrations of SWNTs functionalized with coumarins and coumarin-labeled polymers. (A) coumarin terminated PS, M_n ~2.5k; (B) coumarin terminated PS, M_n ~5k; (C) coumarin terminated PS, M_n ~10k; (D) coumarin-containing block copolymer; (E) coumarin-containing random copolymer; (F) coumarin alone; (G) coumarin and PS.

To obtain these complex structures, novel chromophore-containing polymers were made by SFRP, either using a synthetic chromophore-functionalized monomer or by derivatizing well-defined polystyrenes. The chromophores employed in our investigation were commercially available 7-hydroxycoumarin and coumarin-343. Both of them have high extinction coefficients, high emission quantum yields, and more importantly, single functional groups that are easy to derivatize.

Chapter 3 Results and discussion

3.1 Overview

As discussed in the objectives, the synthesis of coumarin-containing polymers with various structures was the first step to the preparation of soluble SWNT-polymer composites. The following concepts were involved in the synthesis of those polymers: (1) synthesis of polystyrenes in a controlled fashion by SFRP; (2) specific post-functionalization of polystyrenes using designed functional groups at the ends of polymer chains; (3) preparation of a polymerizable coumarin derivative (7-styrylmethoxycoumarin); (4) preparation of 7-styrylmethoxycoumarin random and diblock copolymers. Gel Permeation Chromatography (GPC) measurements (Refractive Index, UV-Vis, and Fluorescence) of the resulting coumarin functionalized polymers provided the molecular weight characteristics and the evidence for the coumarin attachment after post-functionalization, and copolymer formation. ^{1}H NMR analysis provided information about both the molecular weight and the composition of the resulting polymers.

The covalent functionalization of SWNTs with coumarin-containing polymers was done through a radical addition process in DMF at 125 °C. The resulting

SWNT-polymer composites were characterized by IR, NMR, Atomic Force Microspectroscopy (AFM), Transmission Electron Microscopy (TEM), UV-Vis, and Fluorescence spectroscopy. The solubility of the functionalized composites was measured by UV-Vis spectroscopy based on Smalley's method.[37]

3.2 Polystyrene functionalized SWNTs

The first set of experiments was focused on determining whether polymers made by SFRP could be attached to SWNTs via the radical coupling process as discussed in the objectives. In order to address this issue, polystyrene, one of the most common polymers, was used to functionalize shortened SWNTs as a model reaction before we carried out the synthesis of coumarin-containing polymers.

3.2.1 Synthesis and characterization of polystyrene

As mentioned in section 1.3, nitroxide-mediated SFRP is a convenient living polymerization method, especially for styrenics. Functional groups present on each polymer chain are required for post-functionalization of polystyrenes with coumarins. Thus compound **1** (2,2,5,5-tetramethyl-3-(1-phenylethoxy)-4-chloromethyl-phenyl-3-azahexane) was chosen as the initiator (Scheme 4), which was assumed as a good electrophile for S_N2 reactions. It was synthesized

following the procedure reported by Hawker and co-workers.[94] Acetic anhydride was used as an additive for SFRP to obtain a relatively fast polymerization rate and narrow polydispersity.[92,93] The polymerizations were performed in chlorobenzene at 125°C. The resulting polymer products were isolated and purified by precipitation into methanol, filtered and dried in a vacuum oven at 50°C overnight.

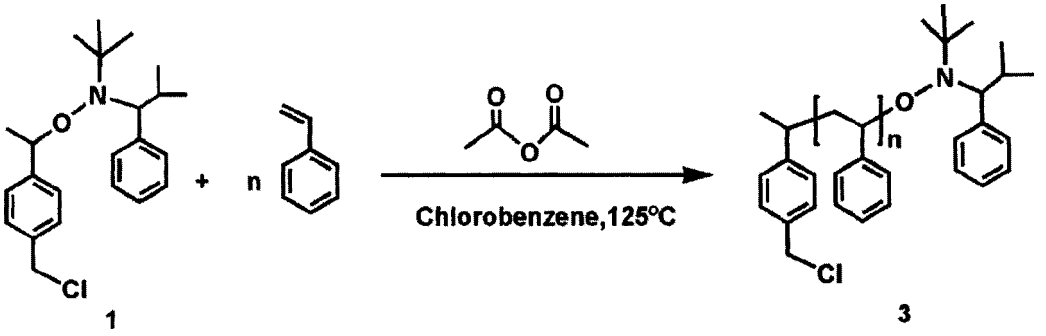

Scheme 4. Homopolymerization of styrene by SFRP.

It was found that this polymerization worked very well even without free nitroxide **2** (Scheme 2), which was typically used in SFRP to control polymerization and maintain a narrow polydispersity. For example, the polystyrene used in the model functionalization reaction of SWNTs was prepared in chlorobenzene at 125°C using nitroxide **1** as the initiator at a 93:1 molar ratio of styrene:**1**. The polymerization time applied was 20 hours, and the final product **3** was analyzed by GPC (M_n = 9693, PDI = 1.08) and NMR. Based on the ^{1}H NMR spectrum of **3** (Figure 9), it is possible to determine the polymer molecular

weight by comparing the integration of signals corresponding to the initiator and the polymer backbone. The resonance at 4.52 ppm is assigned to the chloromethyl group of the initiating chain end. The main peaks at 1.2-2.5 ppm and 6.2-7.4 ppm are assignable to the methine, methylene, and phenyl protons of the polystyrene chain. The molecular weights calculated from NMR (11918) and measured from GPC (9693) are reasonably close, but not identical. The observed difference is due to the fact that both measurements contain some errors: the GPC method is a relative comparison based on a calibration curve, whereas the NMR method relies on accurate measurement of the area under a very small peak. Nevertheless, the reasonable agreement between the two methods was adequate for the structural characterization and for further functionalization reactions.

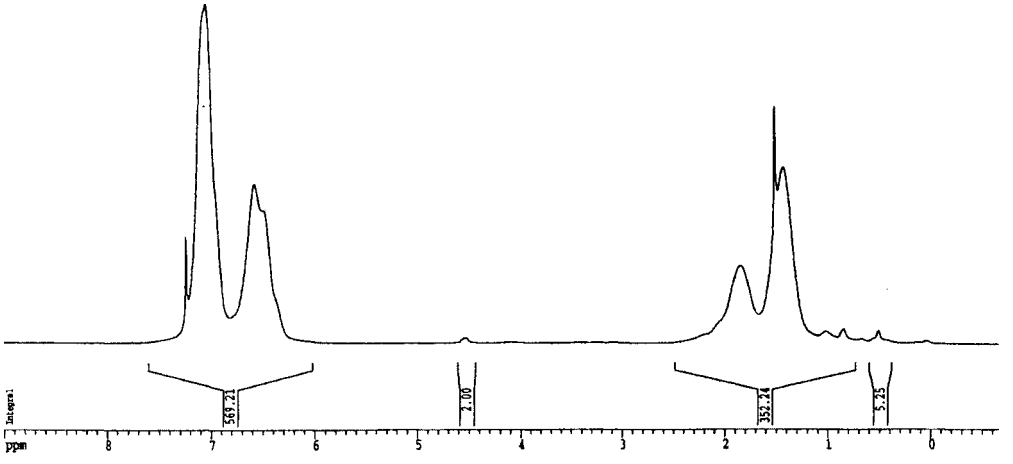

Figure 9. ^{1}H NMR spectrum of PS **3**.

3.2.2 Preparation and characterization of the SWNT-PS composite

Raw SWNT samples made by the HiPco process[95] were purchased from Carbon Nanotechnologies, Inc. Prior to use, they were shortened and purified to yield SWNTs with lengths mostly below 600 nm. Considering the fact that shortened SWNTs were easier to disperse in solvents and had a higher probability of producing soluble structures compared with full-length SWNTs,[41,69] it was important to initially limit the project to appropriately shortened nanotubes. The shortening process was done by sonicating the as-received SWNTs in a mixture of HNO_3/H_2SO_4 following a literature procedure.[43] The shortened SWNTs were then purified by filtration using a polycarbonate membrane having an average pore size of 100 nm, and collected as a black residue left on the membrane. Figure 10 shows the AFM images of carbon nanotubes before and after sonication in HNO_3/H_2SO_4 for 2 hours. It is clear that a substantial length decrease is occurring after 2 hours of sonication.

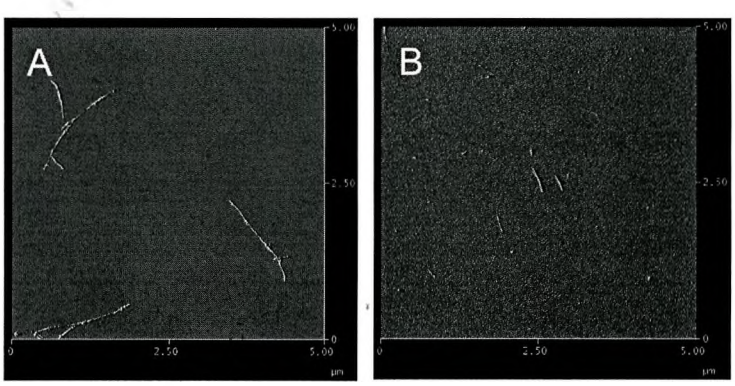

Figure 10. AFM images of as-received SWNTs (A), and SWNTs after sonication for 2 h (B).

Following a procedure developed by Zhaoling Yao in our group, addition of the nitroxide-terminated polystyrene **3** (500 mg) and a catalytic amount of acetic anhydride (50 μL) to a suspension of SWNTs (9.6 mg) in DMF (10 mL), followed by bubbling with N_2 for 30 min and stirring at 125°C under argon for three days, resulted in the functionalized SWNT-PS composite (Scheme 5). After the reaction mixture was cooled down to room temperature, it was filtered through a Teflon membrane with a pore size of 200 nm and washed with a large amount of CH_2Cl_2 (300 mL), $CHCl_3$ (200 mL), and THF (200 mL) until there was no unreacted PS left, as determined by thin layer chromatography (TLC).

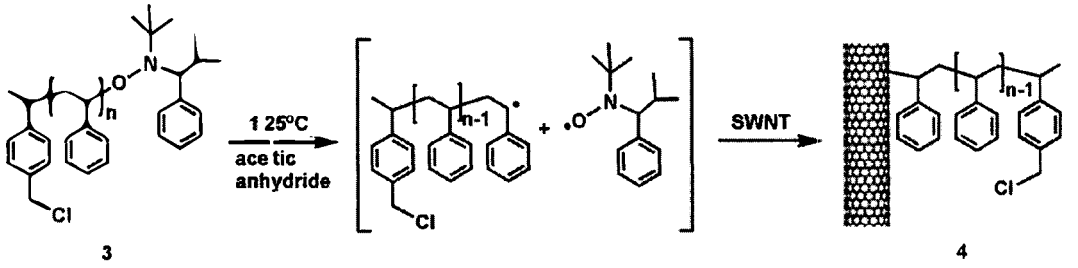

3 4

Scheme 5. Functionalization of SWNTs with PS by radical coupling.

The shortened, unfunctionalized SWNTs were found to be insoluble in common organic solvents, such as CH_2Cl_2, $CHCl_3$, and THF (Figure 11 A-C). After functionalization, however, the product **4** was found to be very soluble in these solvents, as evidenced by the dark color of the solutions (Figure 11 D-F). It has been shown that the concentration of nanotube samples could be determined

by using UV-Vis spectroscopy. Using the specific nanotube extinction coefficient $\varepsilon = 28.6\ cm^2/mg$ at 500 nm reported by Smalley and coworkers,[37] the solubility of the resulting SWNT-PS composite was estimated to be 874 mg/L based on the UV spectrum of 400-fold diluted $CHCl_3$ solution (Figure 12).

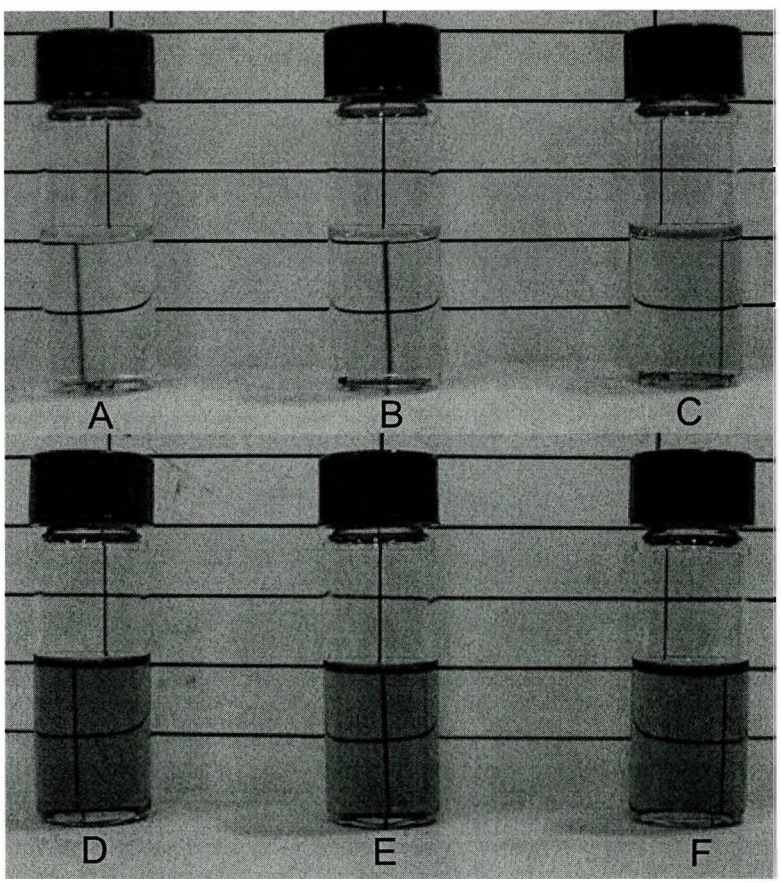

Figure 11. The shortened, unfunctionalized SWNTs in (A) CH_2Cl_2; (B) $CHCl_3$; (C) THF, and solutions of **4** in (D) CH_2Cl_2; (E) $CHCl_3$; (F) THF.

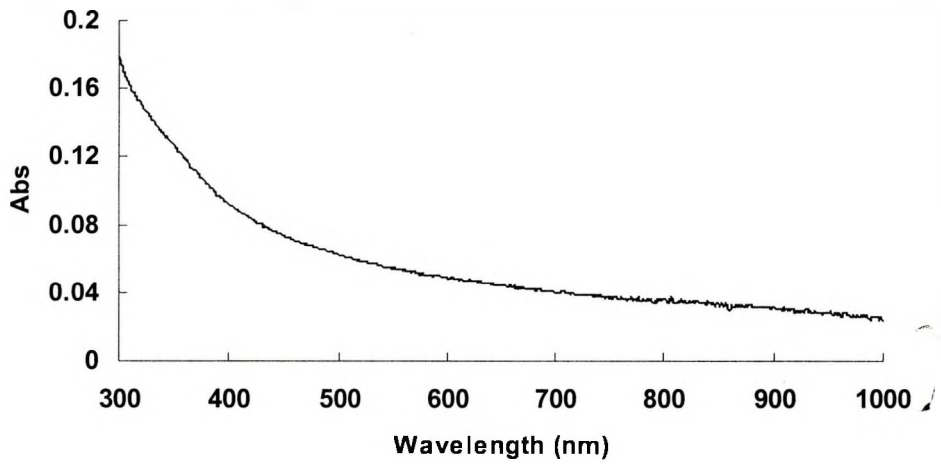

Figure 12. UV-Vis spectrum of PS functionalized SWNTs **4**.

The detailed structural information of **4** was elucidated by solution NMR. Figure 13 presents ^{1}H NMR spectra of the product, SWNT-PS composite **4** and the corresponding starting material, PS **3**. It is clear that these two spectra are quite similar, which suggests the presence of PS in the composite. The broadening of the aromatic proton signals at 7.06 ppm and 6.56 ppm, as well as the aliphatic signals corresponding to the polymer backbone at 1.43 and 1.83 ppm, is attributed to the presence of SWNTs, which lead to a longer relaxation time.

The presence of PS in the resulting SWNT-PS composite **4** could also be confirmed by IR. The IR spectrum of **4** (Figure 14B) is very close to that of **3** (Figure 14A). The peaks at ca. 2929 cm^{-1} and 2856 cm^{-1} represent the aliphatic C-H stretch of the polymer backbone. The peaks in the range from 3100 to 3010 cm^{-1}, as well as those at ca. 1601 cm^{-1}, 1493 cm^{-1}, and 1451 cm^{-1} are

characteristics of aromatic C-H bonds of PS.

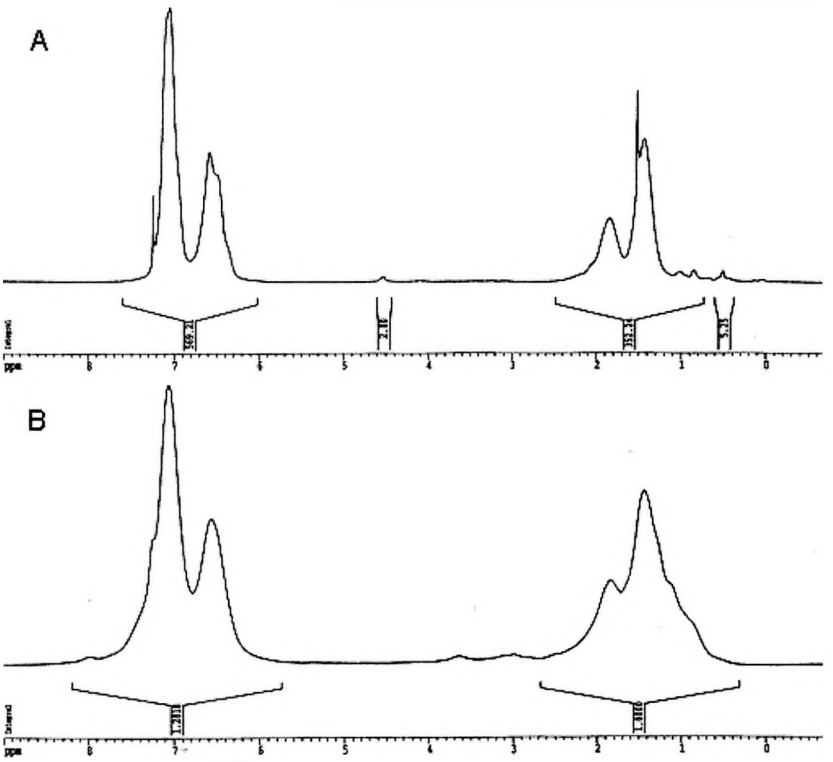

Figure 13. ^{1}H NMR spectra of (A) PS **3**; (B) SWNT-PS composite **4** in $CDCl_3$.

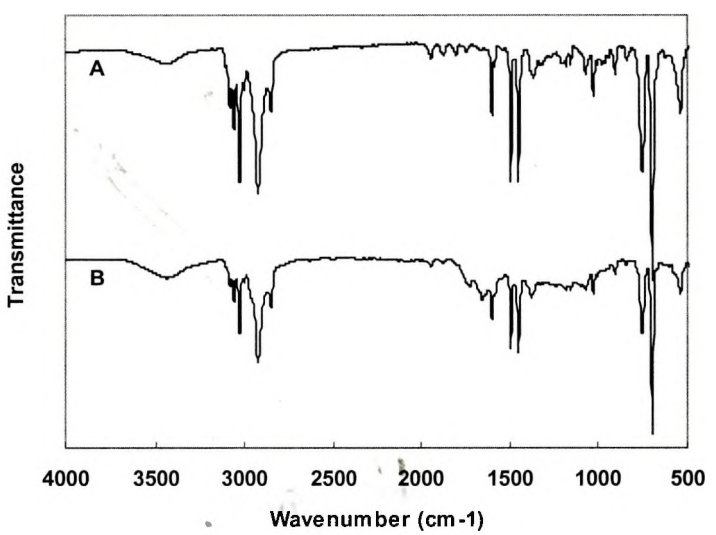

Figure 14. FT-IR spectra of PS **3** (A), and the SWNT-PS composite **4** (B).

To rule out the possibility that PS was just physically absorbed on the surface of SWNTs, a control experiment was previously done, in which the same procedure was carried out except the reaction was done at room temperature rather than 125 °C. Polystyrene remained intact under these conditions. The lack of mass and solubility increase of the final SWNT product was indicative of the fact that polymer coupling did not occur at low temperature and that composite **4** must contain a covalent linkage between the polymer and the SWNTs.

Knowing that polystyrene was present in the composite, AFM was used to show visually that nanotubes were also contained in it. Figure 15 shows the AFM images of the soluble SWNT-PS composite **4** in $CHCl_3$ and THF. In both cases nanotubes are embedded in a polymeric matrix.

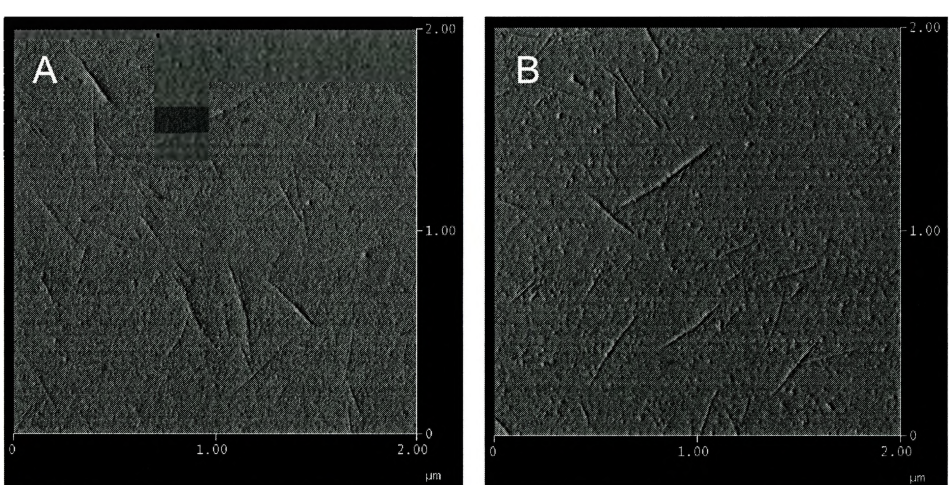

Figure 15. AFM images of **4** in THF (A), and $CHCl_3$ (B).

Samples for AFM measurements were prepared by spincoating the composite solutions onto freshly cleaved mica substrates and the images were recorded with standard tips at a scan rate of 1.0 Hz under tapping mode, which was appropriate for nanotube samples. The lateral force applied to the sample under tapping mode is significantly smaller than that under contact mode. This accounts for why nanotubes on the substrate can remain stationary under tapping mode while they can slide across the surface under contact mode when the tip scans across the substrate. To illustrate this phenomenon, two small square areas (Figure 16) that had been scanned under contact mode were found to be "empty" under tapping mode. This indicates that tips under contact mode have "swept" nanotube samples out of the scanned sections, illustrating that this scanning procedure is not suitable for properly imaging the nanotube samples.

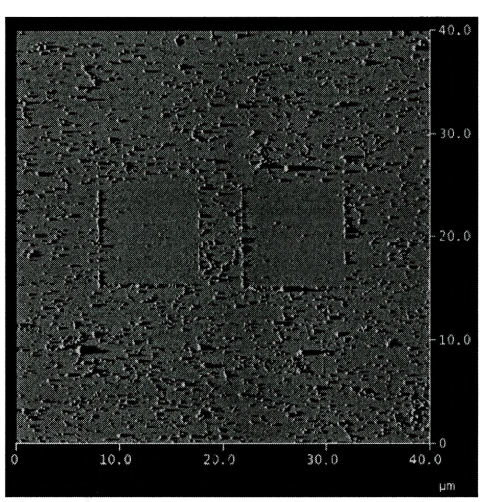

Figure 16. AFM image of as-received SWNTs under tapping mode for a large area including two square areas that have been scanned in contact mode.

3.3 7-Hydroxycoumarin terminated PS functionalized SWNTs

Two possible ways could be envisioned to carry out the functionalization of SWNTs with coumarin-terminated polystyrenes. One is first to functionalize SWNTs with PS as the model reaction, then attach coumarins to the nanotube-PS composites; the other is first to prepare coumarin-terminated polystyrenes, and then perform the radical functionalization of SWNTs. In the former case, nanotubes are involved in two reaction steps. In the latter case, only one step of the reaction sequence involves the nanotubes. Additionally, in the latter case, chromophore-functionalized polymers can be well characterized prior to nanotube coupling. Therefore the second route was chosen for the preparation of the 7-hydroxycoumarin terminated PS functionalized SWNT composite.

3.3.1 Preparation and characterization of 7-hydroxycoumarin functionalized PS

The post-functionalization concept was used in the synthesis of coumarin-functionalized polystyrene by taking advantage of the chloromethyl group at the polystyrene chain end. It was found that the chloromethyl groups were still very reactive for Williamson Ether Synthesis after the polymer chain was formed. The post-functionalization reactions of PS are shown in Scheme 6.

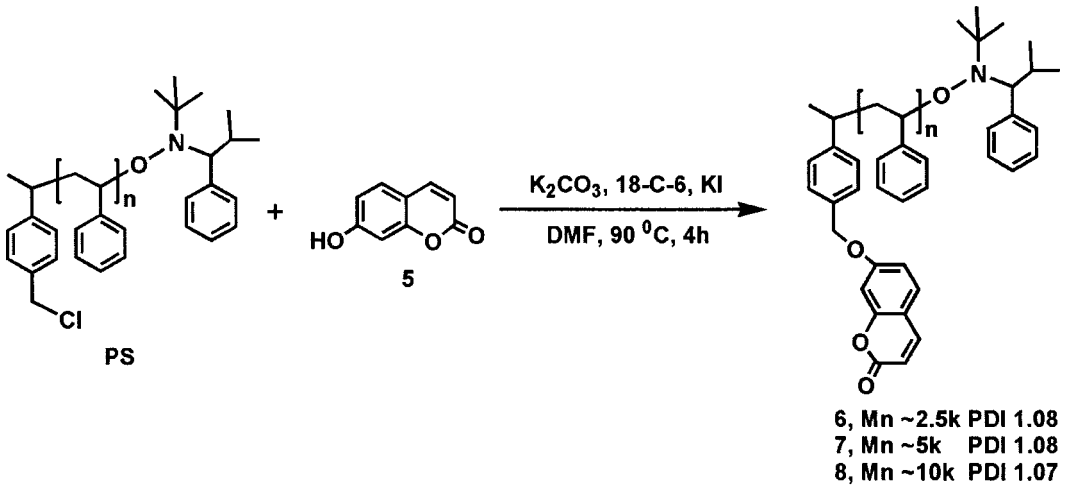

Scheme 6. Synthesis of 7-hydroxycoumarin terminated PS.

Heating of a mixture of PS, 7-hydroxycoumarin **5**, potassium carbonate, 18-crown-6, and a catalytic amount of potassium iodide in DMF for 4 hours led to the formation of coumarin functionalized polystyrene (**6, 7, 8**). The reactions were monitored by TLC and the final products were purified by column chromatography using 5/5 EtOAc/Hexanes as the eluent, followed by precipitation into methanol. After drying in a vacuum oven at 50 °C overnight, the products were obtained as a white powder. The high efficiency of these reactions was demonstrated by the short reaction time as well as relatively high yields (all over 82% even after extensive purification). ^{1}H NMR was utilized to confirm the complete conversion of chloromethyl groups into ether linkages.

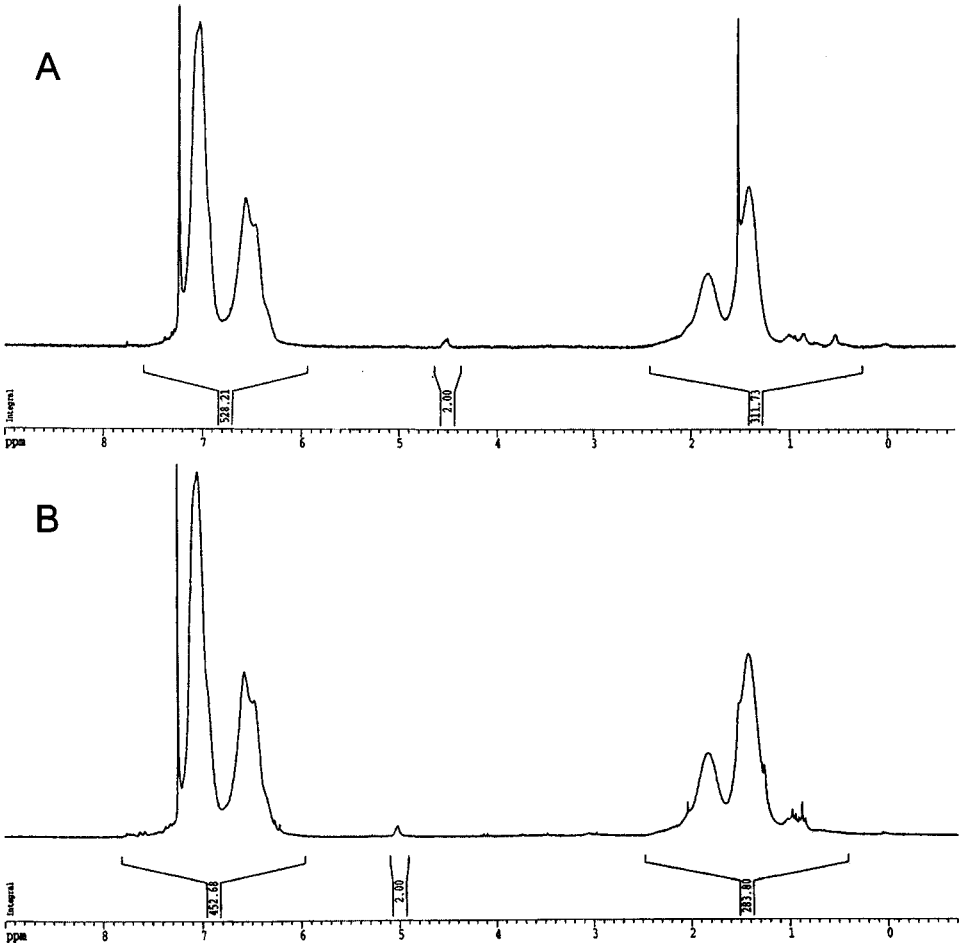

Figure 17. ^{1}H NMR spectra of PS (A), and **8** (B).

The signal corresponding to chloromethyl group of starting material, PS at 4.5 ppm (Figure 17A) completely disappeared after the post-functionalization, which produced a related signal at 5.0 ppm (Figure 17B). The complete conversion is very important since it would be difficult to determine the composition of the resulting nanotube composites if unreacted PS was left.

The successful attachment of coumarin units to PS can also be confirmed by

IR spectra. Upon conversion of PS (Figure 18A) to **7** (Figure 18B), the IR spectrum exhibits the expected absorption band centered at ca. 1744 cm^{-1}, which is characteristic of ester carbonyl groups.

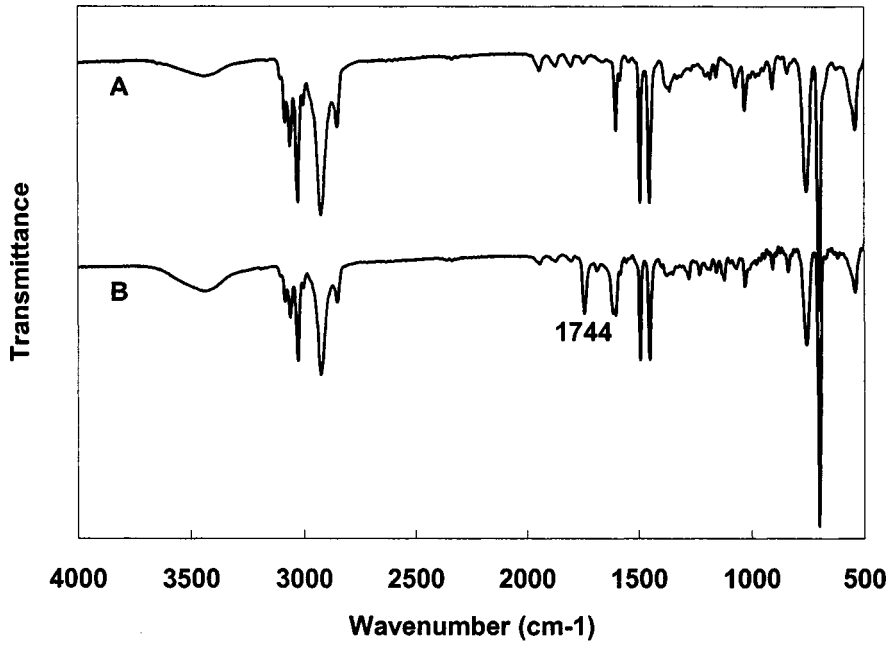

Figure 18. FT-IR spectra of PS (A), and **7** (B).

As 7-hydroxycoumarin is fluorescent (λ_{max} 325 nm, λ_{em} 390 nm), GPC analysis with a fluorescence detector was also employed to ensure that 7-hydroxycoumarin had been successfully incorporated into PS chains. Figure 19 illustrates the fluorescence chromatograms of coumarin-attached polystyrenes as a function of elution time. For this analysis, the excitation wavelength was 325 nm and emission wavelength was 390 nm. All three polymers **6**, **7**, and **8** showed

significant fluorescence where pure PS showed no fluorescence. The fluorescence peaks of these three polymers match well with their RI traces, which indicates that all of these three different post-functionalized polymers have incorporated 7-hydroxycoumarin **5** into them.

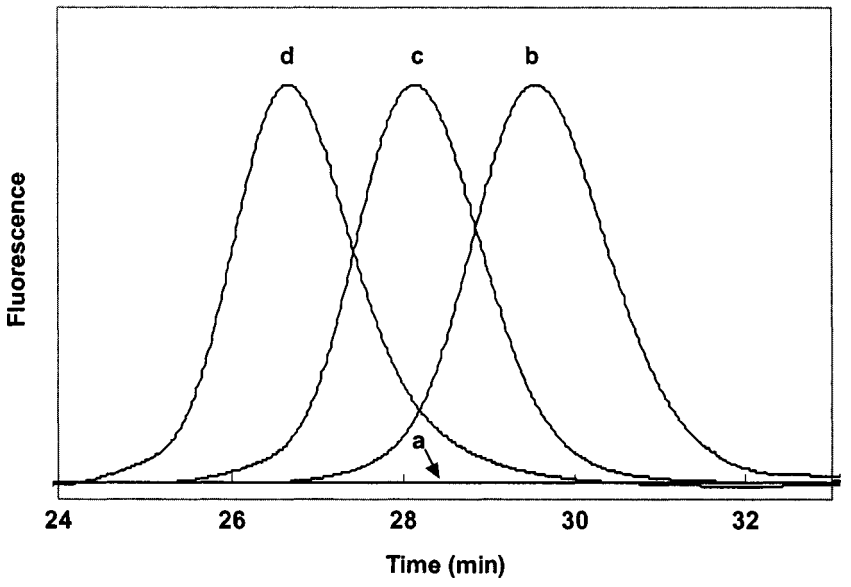

Figure 19. Comparison of fluorescence curves for (a) PS M_n ~4.5k; (b) Coumarin-PS **6** M_n ~2.5k; (c) Coumarin-PS **7** M_n ~5k; (d) Coumarin-PS **8** M_n ~10k.

All of these measurements confirmed that the designed coumarin-terminated polymers were prepared.

UV-Vis spectroscopy was utilized to determine the effect of conversion of the hydroxyl group to an ether linkage on the UV/Vis absorbance due to the presence of the coumarin unit. It was found that the wavelength of maximum absorbance

shifted from 318 nm for 7-hydroxycoumarin to 322 nm for coumarin-PS **7** (Figure 20). The strong absorbance at 254 nm in Figure 20b is attributed to the characteristic phenyl absorbance of the styrene repeating unit.

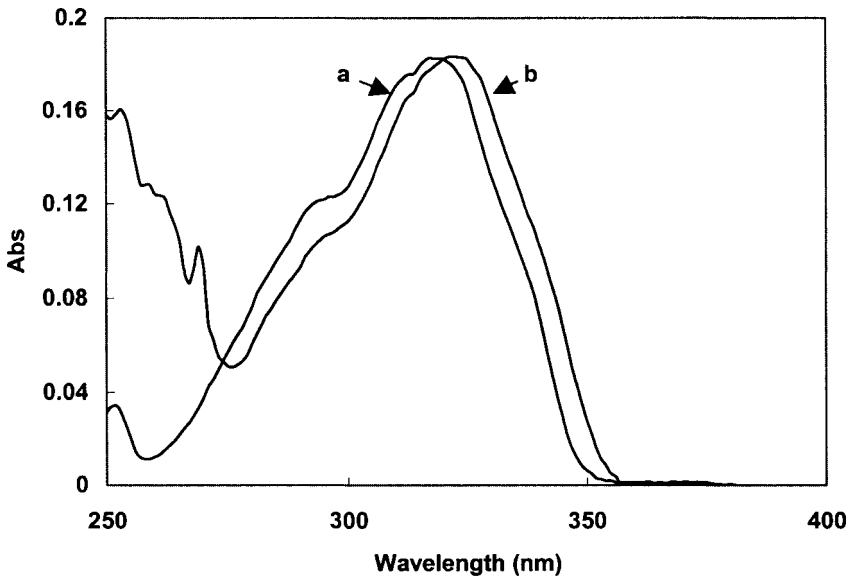

Figure 20. Normalized UV-Vis spectra of 7-hydroxycoumarin (a), and coumarin-PS **7** (b) in CH_2Cl_2.

Figure 21 illustrates the emission spectra of the resulting coumarin-terminated polymer **7** (λ_{em} 391 nm) and 7-hydroxycoumarin (λ_{em} 390 nm) with excitation at 320 nm, all normalized at the UV absorbance of 320 nm. It is clear that the conversion of the hydroxyl group to an ether linkage resulted in a significantly increased quantum yield.

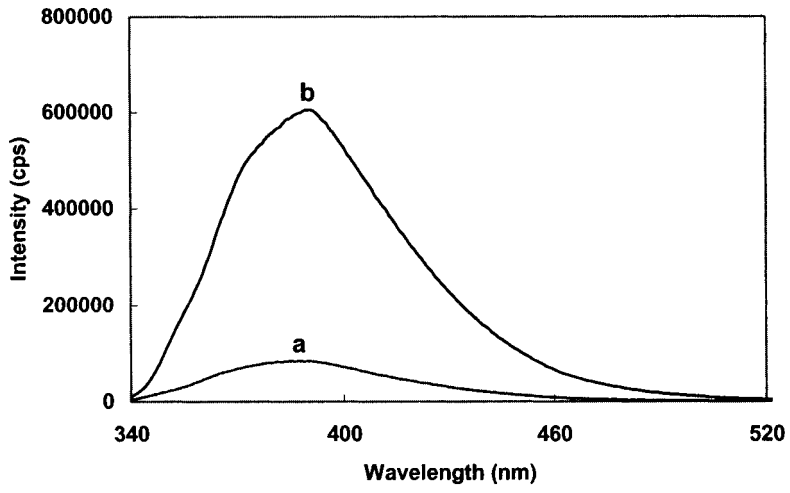

Figure 21. Overlay of normalized emission spectra for 7-hydroxycoumarin (a), and coumarin-PS **7** (b) in CH_2Cl_2.

3.3.2 Preparation and characterization of SWNT-PSOCoumarin composites

The method for the preparation of 7-hydroxycoumarin terminated PS functionalized SWNTs (SWNT-PSOCoumarin) **9**, **10**, and **11** (Scheme 7) was the same as the one employed for the SWNT-PS composite. This involved bubbling in DMF with N_2 for 30 min and heating at 125 °C for 3 days. The reactions were then worked up by filtration using a 200 nm pore Teflon membrane. The residue on the membrane was washed with CH_2Cl_2, THF, and $CHCl_3$ to remove acetic anhydride, free nitroxide formed in these reactions, and unreacted polymers. The complete removal of any unreacted small molecules and polymers was confirmed

by TLC. After the residues were dried in a vacuum oven at 50 °C overnight, a black solid was isolated. The mass increase of these resulting composites was about 30%.

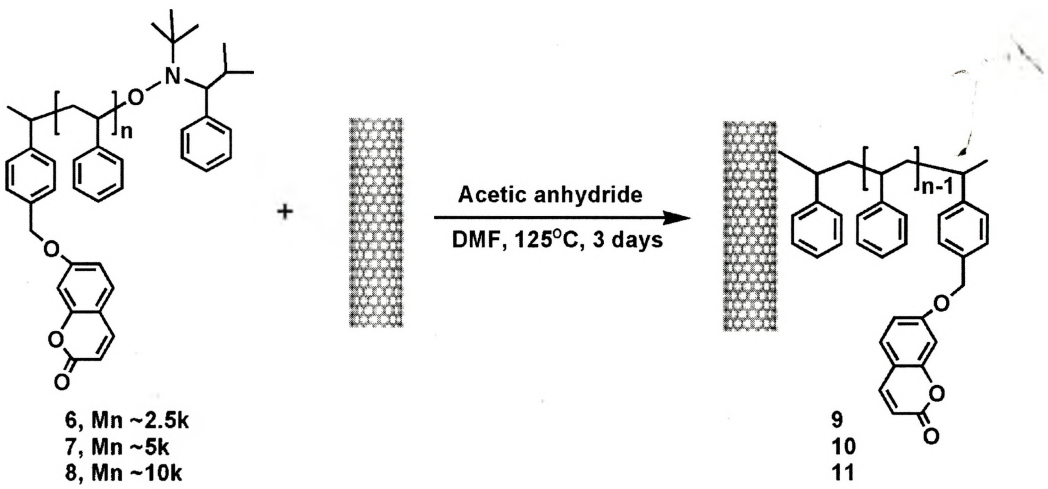

Scheme 7. Functionalization of SWNTs with coumarin-PS by radical coupling.

This functionalization reaction was followed by IR spectroscopy. The spectrum of the unfunctionalized SWNTs is shown in Figure 22A, which exhibits the expected C=O stretch at 1741 cm^{-1} arising from the carboxylic acid groups introduced as a result of the shortening process. The large IR band observed at 3400 cm^{-1} and the weak one at 1632 cm^{-1} are attributed to the asymmetrical stretching and scissoring vibrations, respectively, due to traces of water in the KBr pellet used for the analysis. After functionalization, the attachment of the polymer was illustrated by the appearance of aliphatic C-H stretchs (2980 to 2920

cm^{-1}) and aromatic C-H stretches (3110 to 3020 cm^{-1}), and the appearance of a strong C=O stretch (1729 cm^{-1}) from the coumarin ester linkage (Figure 22B).

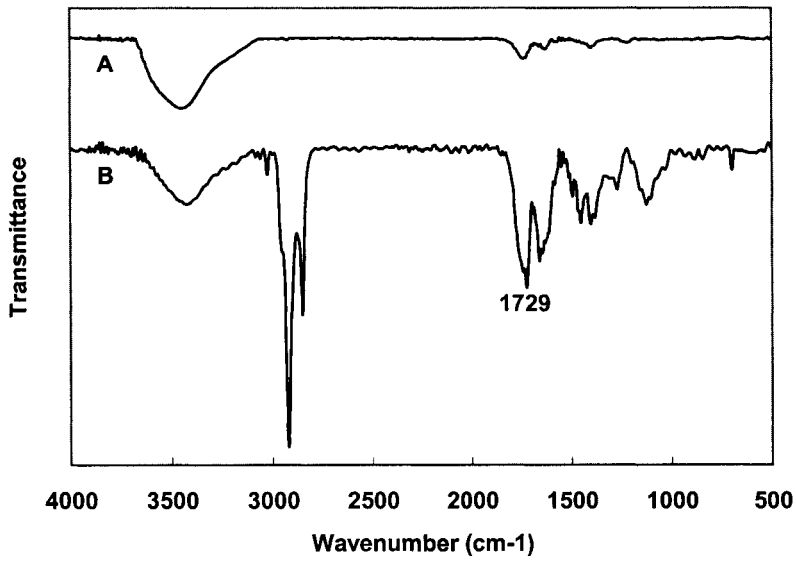

Figure 22. IR spectra for the shortened, unfunctionalized SWNT (A), and **9** (B).

It was found that **9**, **10**, and **11** were all soluble in chloroform, but insoluble in CH_2Cl_2 and THF. Figure 23 shows the photograph of these coumarin-PS functionalized SWNT composites' solutions in $CHCl_3$. For comparison, the starting material, shortened SWNTs in $CHCl_3$ is also presented. The solutions of these functionalized composites in $CHCl_3$ were quite dark while the liquid layer of shortened SWNT in $CHCl_3$ remained colorless, which is consistent with pristine SWNTs being insoluble in common organic solvents. Among these composites, **10** was found to be the most soluble in $CHCl_3$.

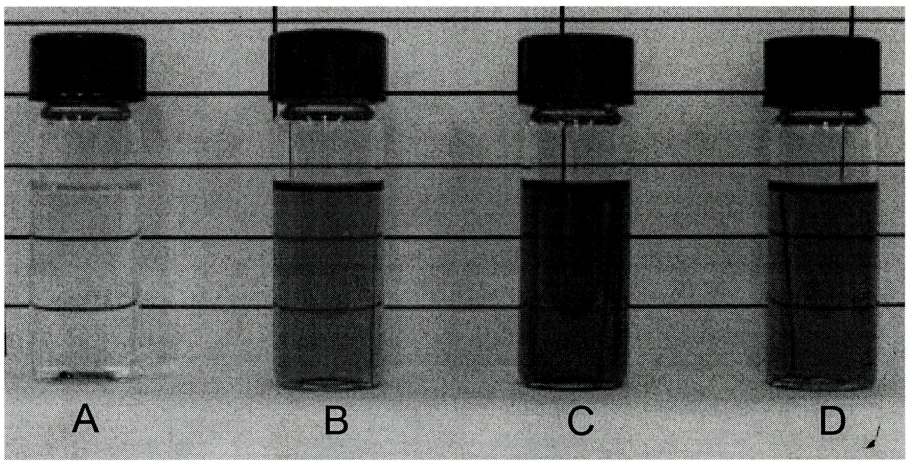

Figure 23. (A) Shortened SWNTs in $CHCl_3$ and Solutions of SWNT-PS-Coumarin composites (B) **9**; (C) **10**; (D) **11** in $CHCl_3$.

To make sure the ether linkage was stable at 125 °C even after three days, the free polymer in the filtrate from the washing step was isolated by precipitation into methanol twice and analyzed by ^{1}H NMR and GPC. The signal at 5.0 ppm (Figure 24), resulting from the diagnostic methylene protons by the ether bond of **8** was still present in the spectrum of the recovered polymer, indicating that the coumarin end group remained intact. Both of M_n (8597) and PDI (1.08) for the recovered polymer are very close to those of the original polymer, 8804 and 1.07 respectively, which suggests that polymer radical coupling did not happen during this process. It should be noted that in a control experiment, in which only the SFRP initiator **1** was used to perform the same process, the product was insoluble. This means the solubility of **9**, **10** and **11** was due to the presence of the coumarin-terminated polystyrenes.

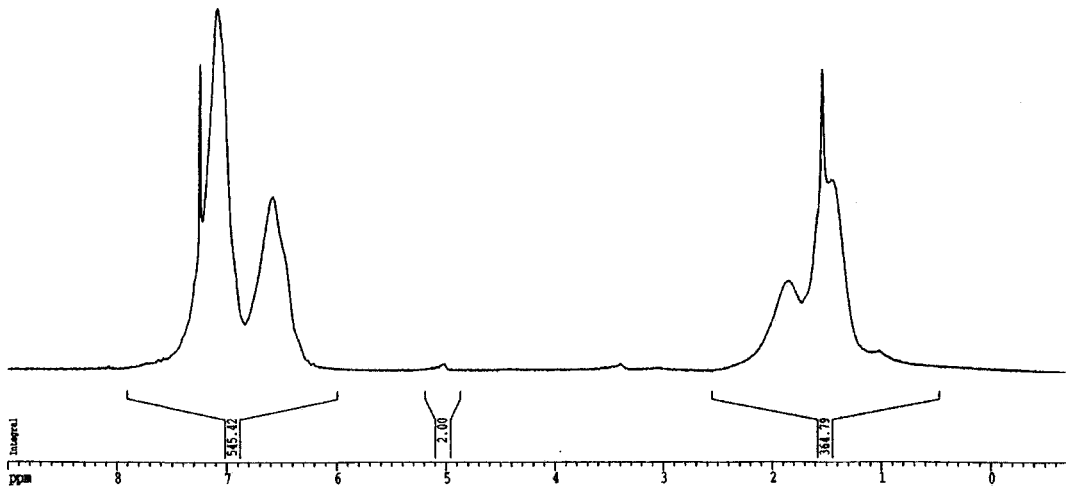

Figure 24. ^{1}H NMR spectrum of **8** in $CDCl_3$ after coupling reaction.

The morphology of these polymer-functionalized nanotubes was studied using AFM. Figure 25 shows the AFM images of the resulting polymer functionalized SWNTs spin-coated from chloroform solutions onto mica substrates. Compared with shortened SWNTs, which typically have average heights below 4.5 nm, many of these polymer-SWNT composites have average heights over 6 nm. Some of the individual features along the nanotubes reach up to 13 nm in height, indicating that nanotubes were not evenly functionalized.

Polymer functionalized SWNTs were also observed by TEM (Figure 26). Samples were prepared by dispersing solutions of SWNT-polymer composites onto a holey carbon-coated copper grid. These samples produced a film in which it was possible to discern embedded SWNTs. Upon irradiation with the electron

beam, the polymer film became closely associated with the nanotube skeleton to produce structures in which individual nanotubes and small nanotube bundles were sheathed by regions of amorphous carbon, presumably corresponding to the polymer portion of the composites. In some areas, these sheathed structures were found to contain gaps that were bridged by SWNTs.

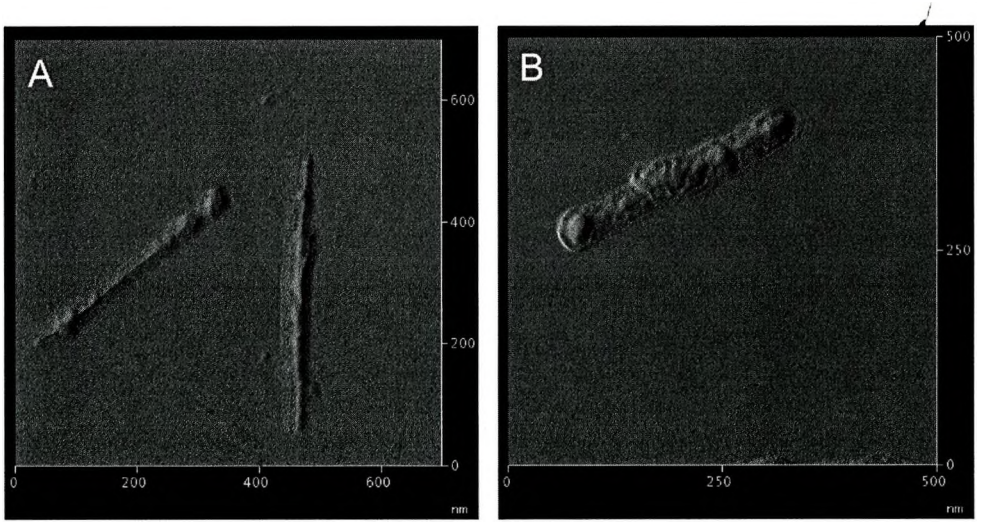

Figure 25. AFM images of **9** (A), and **10** (B) in $CHCl_3$.

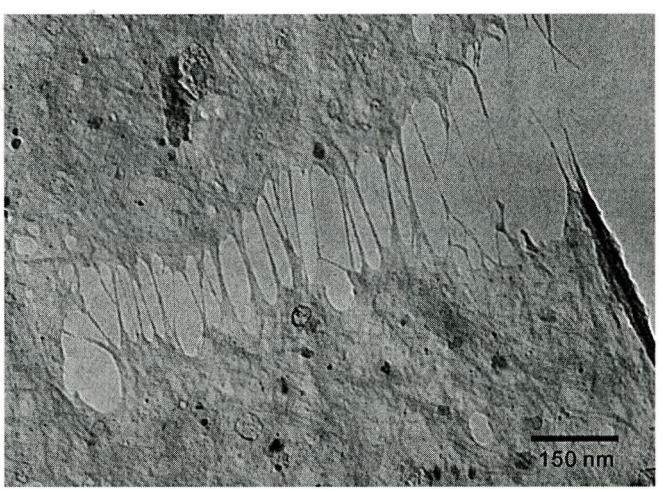

Figure 26. TEM micrograph of **11**.

Figure 27 illustrates the absorbance properties of the resulting coumarin-polymer functionalized SWNT composites, all normalized to their absorbance at 500 nm. The absorption bands around 320 nm, corresponding to coumarin absorption, were not clearly visible due to the relatively low density of coumarin units in the nanotube composites, and the overwhelmingly strong absorption arising from the nanotubes. For each of the nanocomposites, the absorption spectra are extremely similar, indicating no major difference in electronic structure resulting from changes in polymer chain length.

Figure 28 depicts the emission spectra of these composites, as well as that of coumarin terminated PS **6**, all normalized at 391 nm (λ_{em}). It should be noted that the emission spectra of polymers **7** and **8** are identical to that of **6,** after normalization. Interestingly, although the absorption spectrum of the coumarins could not be discerned from that of the nanotubes, the emission spectra clearly exhibit coumarin fluorescence. Furthermore, the nanotube-tethered coumarins seem to have broadened emission spectra, where broadening increase as the polymer length decreases. This trend may be indicative of electronic interactions between the chromophores and the nanotubes. As the polymer chain length decreases, the degree of chromophore-nanotube interaction should increase, possibly resulting in the observed spectral broadening.

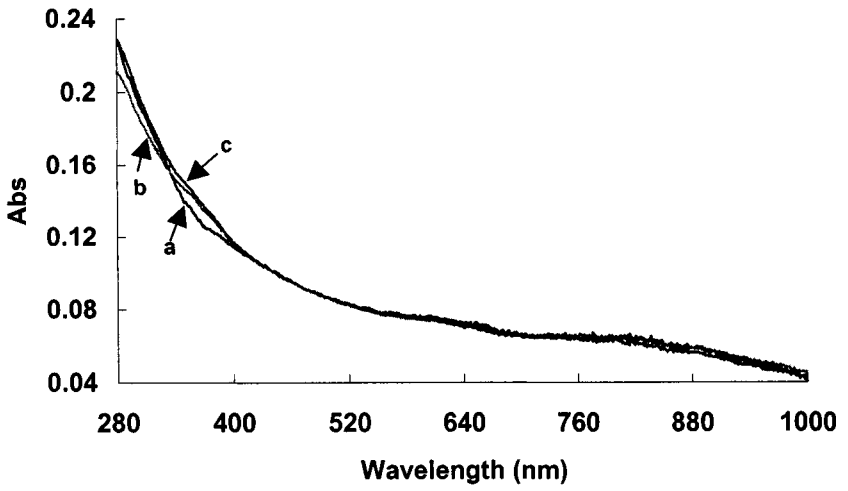

Figure 27. UV-Vis spectra of **9** (a), **10** (b), and **11** (c) in $CHCl_3$.

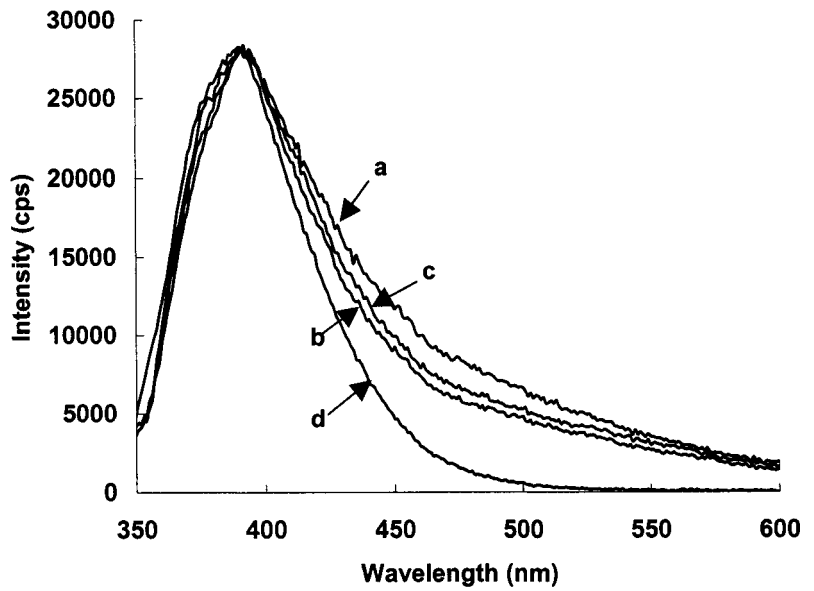

Figure 28. Overlay of normalized emission spectra for **9** (a); **10** (b); **11** (c) in $CHCl_3$, and **6** (d) in CH_2Cl_2.

3.4 Poly[styrene-*co*-(7-styrylmethoxycoumarin)] functionalized SWNTs

In order to determine the effect of multiple chromophores on the absorbance and emission properties of SWNTs, diblock copolymers were used to functionalize SWNTs, in which the first block was PS designed to increase the solubility, and the second block contained 7-hydroxycoumarin bonded to the nitroxide group. As a comparison, a random copolymer with the same components as block copolymers was also synthesized and employed to functionalize SWNTs.

3.4.1 Synthesis and characterization of 7-hydroxycoumarin containing monomer

To ensure that the living free radical chain extension occurs smoothly, and more importantly, the subsequent functionalization of SWNTs occurs efficiently, it is preferable for the co-monomer to have similar reactivity to that of styrene. We therefore chose 7-styrylmethoxycoumarin to carry out the task outlined above. 7-styrylmethoxycoumarin **13** was obtained as shown in Scheme 8. Refluxing 4-vinylbenzyl chloride **12** in a mixture of 7-hydroxycoumarin **5**, potassium carbonate, 18-crown-6 and a catalytic amount of potassium iodide in acetone for 4.5 hours led to the formation of monomer **13**. The reaction was monitored by

TLC and the final product was purified by column chromatography using CH_2Cl_2 as the eluent. After drying under vacuum overnight, a white powder (91% yield) was obtained.

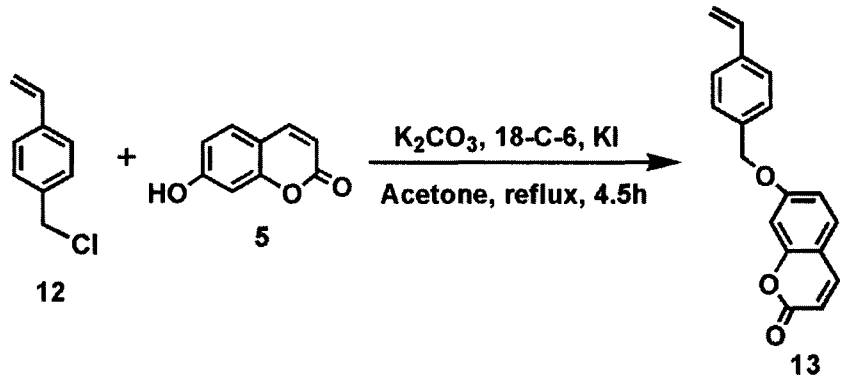

Scheme 8. Synthesis of 7-styrylmethoxycoumarin.

Mass spectrometry, ^{1}H NMR, and ^{13}C NMR were utilized to characterize the product. Mass spectrometry (Figure 29) gave a molecular weight of 278.1 Da, exactly matching the expected molecular weight of monomer **13**. The peak assignments and integrations of the ^{1}H NMR spectrum (Figure 30) were consistent with the structure of **13**. The diagnostic methylene protons next to the ether linkage appear at 5.10 ppm, and the three vinyl protons appear at 5.26, 5.75 and 6.71 ppm. Monomer **13** showed signals at 101.4-161.0 ppm for the sp^2 carbons in ^{13}C NMR (Figure 31). The resonance at 161.8 ppm is characteristic for the ester C=O moiety. The signal at 70.3 ppm is diagnostic for the methylene carbon. These results indicate that the desired monomer was obtained.

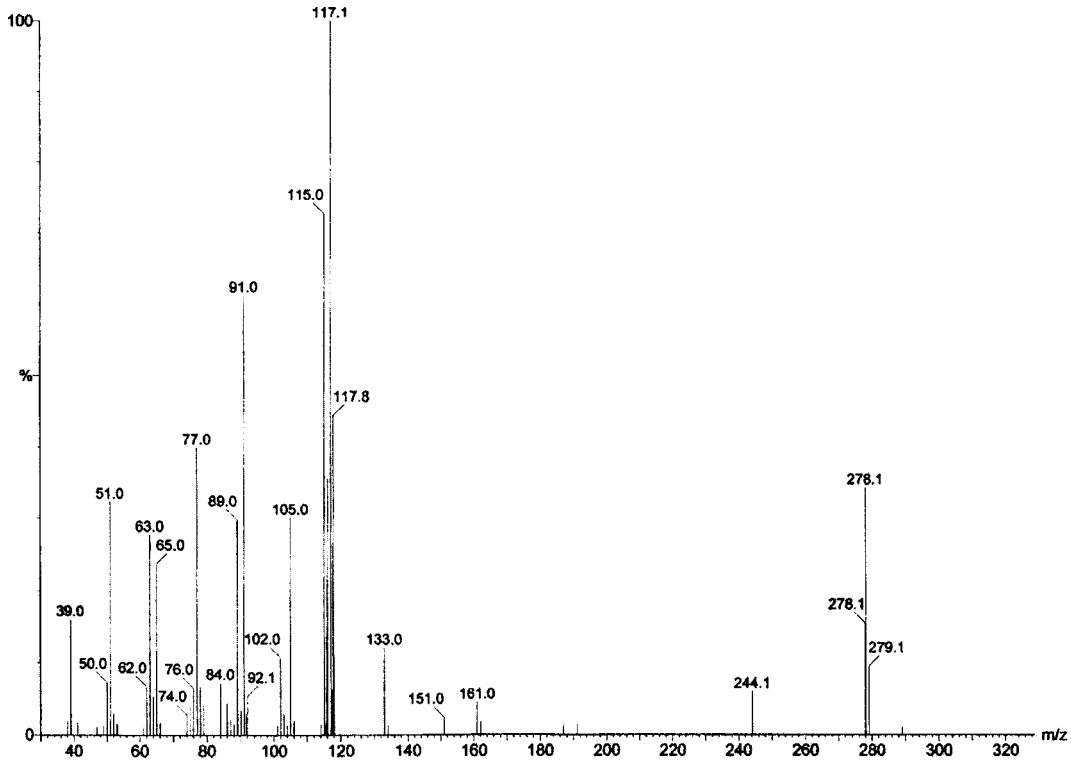

Figure 29. Mass spectrum of monomer **13**.

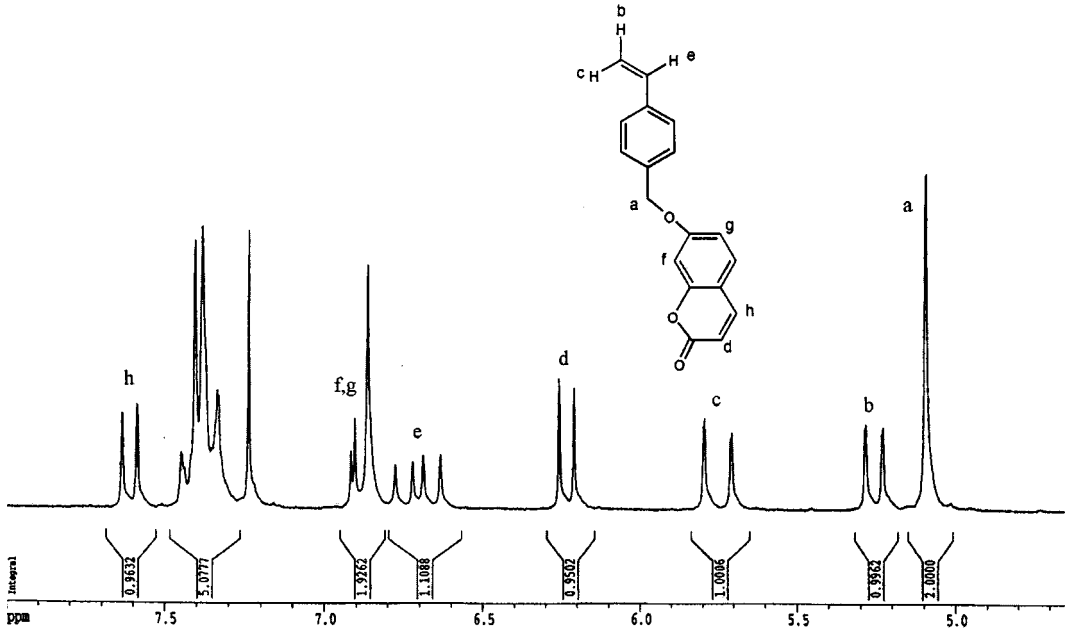

Figure 30. ^{1}H NMR spectrum of monomer **13** in $CDCl_3$.

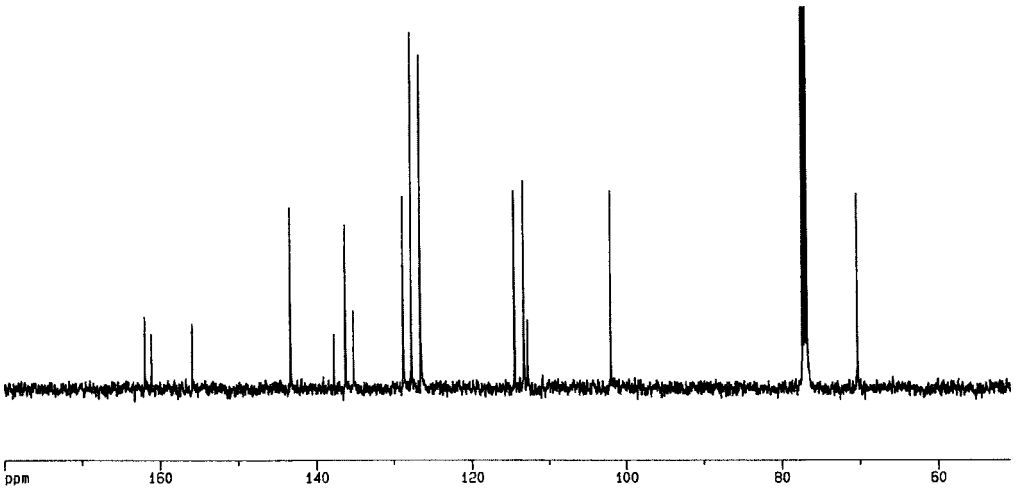

Figure 31. ^{13}C NMR spectrum of monomer **13** in $CDCl_3$.

3.4.2 Preparation and characterization of Poly[styrene-*b*-(7-styrylmethoxycoumarin)]

The first series of experiments were focused on determining whether the chain extension of PS (M_n = 5164, PDI = 1.08) with this synthetic monomer **13** could work, as exhibited in Scheme 9. The initial test reaction was performed in DMF at 125°C using nitroxide terminated PS as the macroinitiator at a 15:1 molar ratio of **13**:PS. Aliquots taken from the reaction mixture at various reaction times were analyzed by GPC to ensure chain extension had occurred so far. The resulting GPC curves using a refractive index detector shown in Figure 32 indicated that monomer **13** was polymerized and the molecular weight of the block copolymers increased with the polymerization time. Beyond 2 hours, however, the reaction extent changed very little.

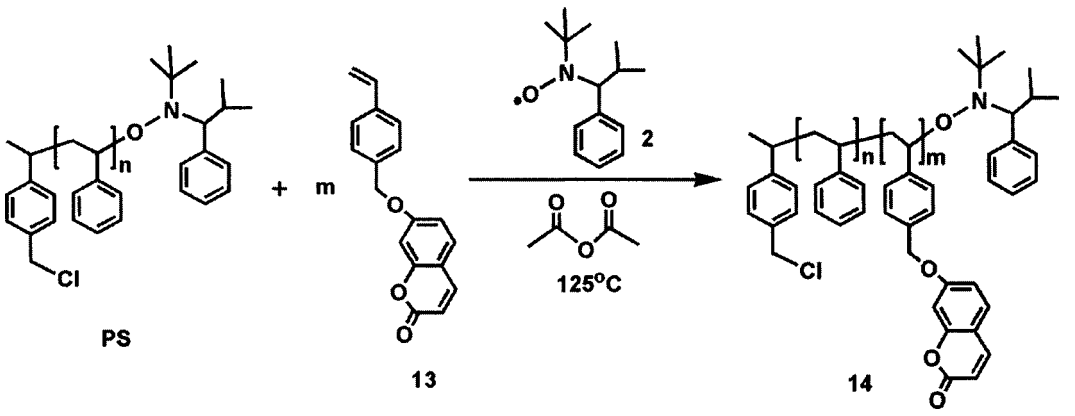

Scheme 9. Preparation of poly[styrene-*b*-(7-styrylmethoxycoumarin)].

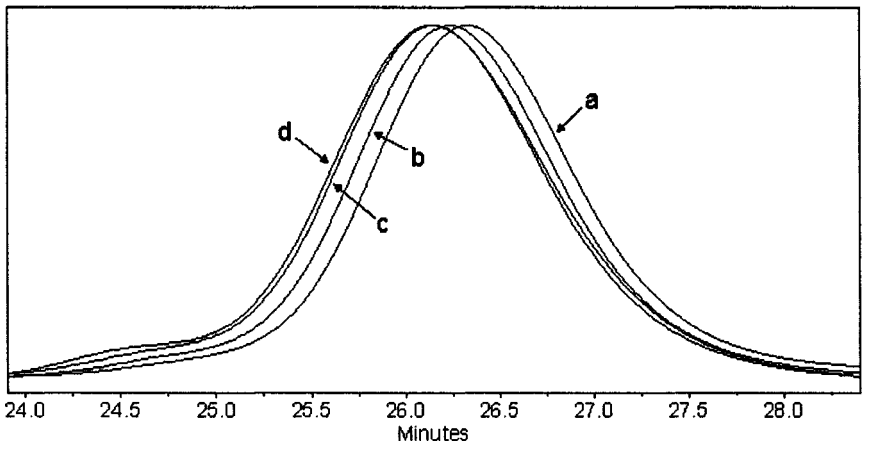

Figure 32. GPC traces of (a) macroinitiator PS (M_n = 5164, PDI = 1.08), and chain extension products at various polymerization times (b) 1 h (M_n = 5393, PDI = 1.07); (c) 2 h (M_n = 5598, PDI = 1.09); (d) 4 h (M_n = 5618, PDI = 1.09).

Knowing that chain extension of PS with monomer **13** is feasible, a more precise coumarin containing block copolymer **14** was obtained by polymerizing the mixture of monomer **13** and PS (M_n = 5449, PDI = 1.12) at a 10:1 molar ratio of **13** to PS in DMF at 125°C for 1 hour. The product was purified by column chromatography using 5/5 Hexanes/EtOAc followed by pure EtOAc as the eluents.

The final product **14** was analyzed by both GPC (M_n = 8493 g/mol, PDI = 1.15) and NMR measurements. Based on its ^{1}H NMR spectrum (Figure 33), the number of attached coumarin units was determined to be 20 by comparing the integration areas of signals corresponding to the protons next to the ether linkage and the protons by the chlorine atom.

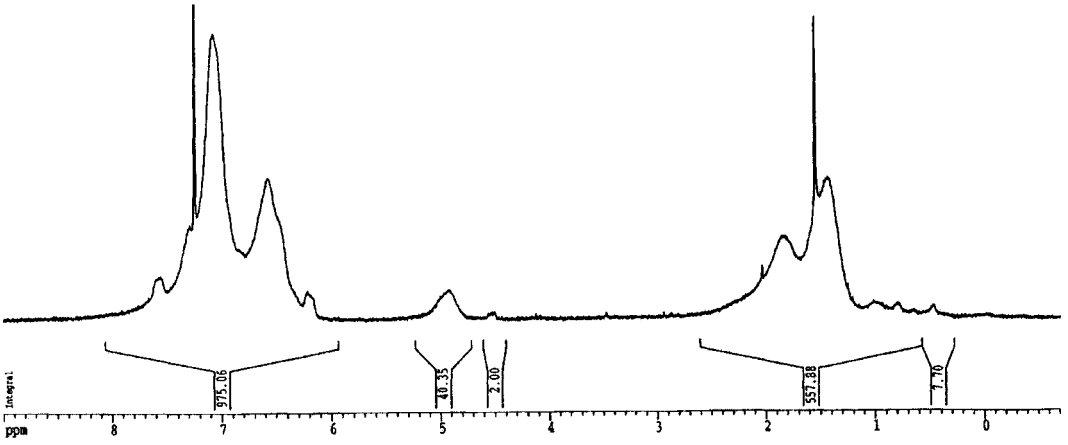

Figure 33. ^{1}H NMR spectrum of block copolymer **14** in $CDCl_3$.

3.4.3 Preparation and characterization of Poly[styrene-*r*-(7-styrylmethoxycoumarin)]

In order to understand what difference the distribution of multiple chromophores along the polymer chains might cause, a random copolymer **15**, with the same two components as the block copolymer was made and utilized to functionalize SWNTs. It was obtained by polymerizing the mixture of monomer **13** and styrene at a 1:6 molar ratio of **13** to styrene in DMF at 125°C using **1** as

the initiator (Scheme 10). After precipitation into methanol twice, unreacted monomers were completely removed, which was confirmed by TLC and GPC using a fluorescence detector. It was then analyzed by GPC (M_n = 4254 g/mol, PDI = 1.33). As in the case of the block copolymer, the number of coumarin units in this copolymer (**p**) was determined by ^{1}H NMR to be approximately 8. This was calculated by comparing the integrated area of the peak corresponding to the protons by ether linkage and the protons by the chlorine atom.

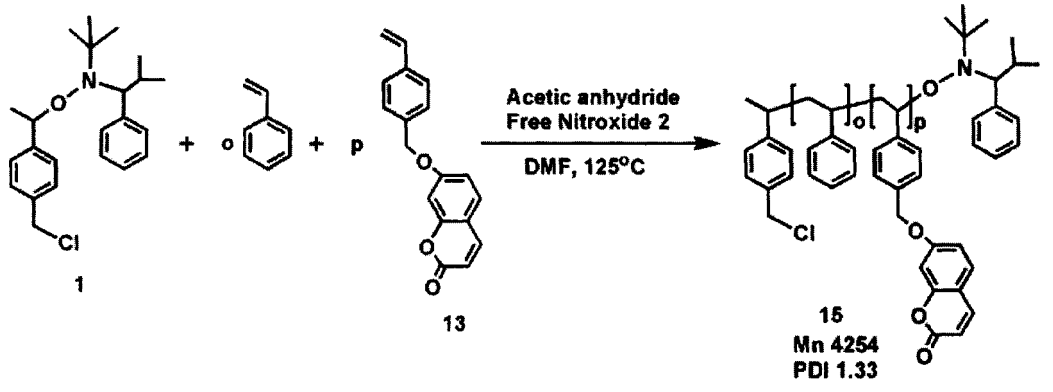

Scheme 10. Preparation of poly[styrene-*r*-(7-styrylmethoxycoumarin)].

3.4.4 Preparation and characterization of coumarin-containing copolymer functionalized SWNT composites

The synthesis of poly[styrene-*b*-(7-styrylmethoxycoumarin)] functionalized SWNT composites **16**, and poly[styrene-*r*-(7-styrylmethoxycoumarin)] functionalized SWNT composites **17** is presented in Scheme 11. The same conditions for polymer nanotube coupling as described previously were applied

including bubbling with N_2 for 30 minutes, heating at 125 ^{o}C for three days, followed by filtration and washing with $CHCl_3$, THF and CH_2Cl_2. TLC was used to confirm the absence of any unreacted polymers in the final products.

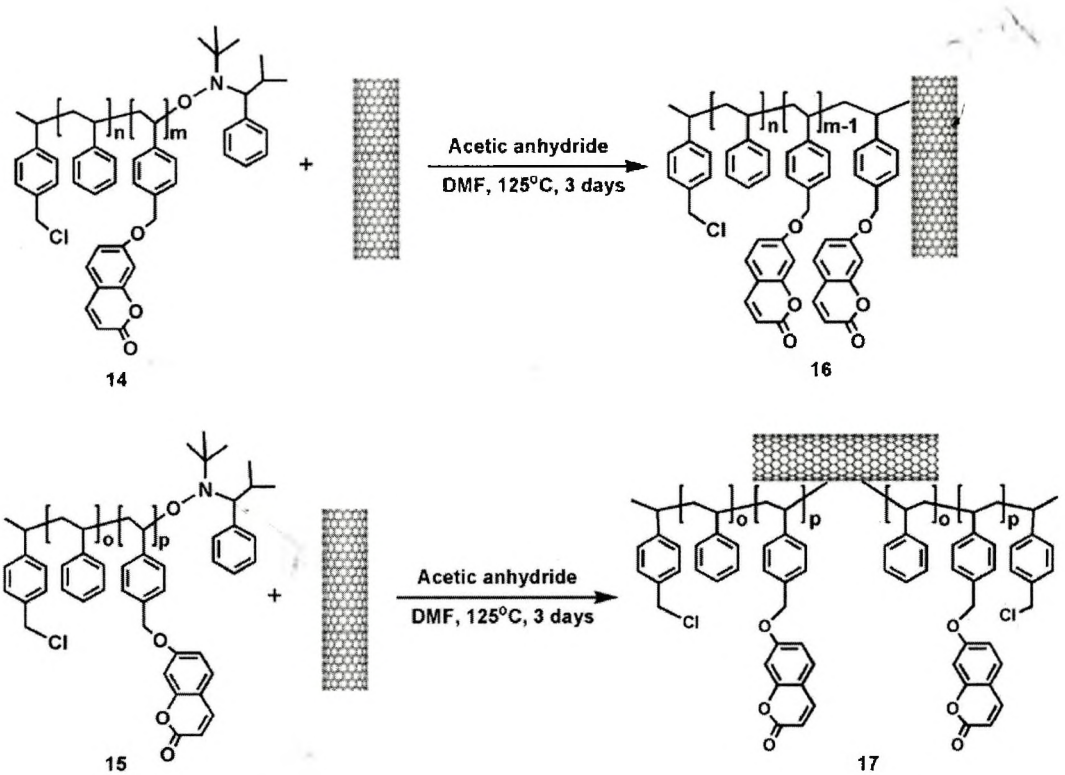

Scheme 11. Functionalization of SWNTs with coumarin containing block copolymer and random copolymer.

Both **16** and **17** were found to be soluble in $CHCl_3$ (Figure 34B & C), while the shortened unfunctionalized SWNTs were completely insoluble (Figure 34A).

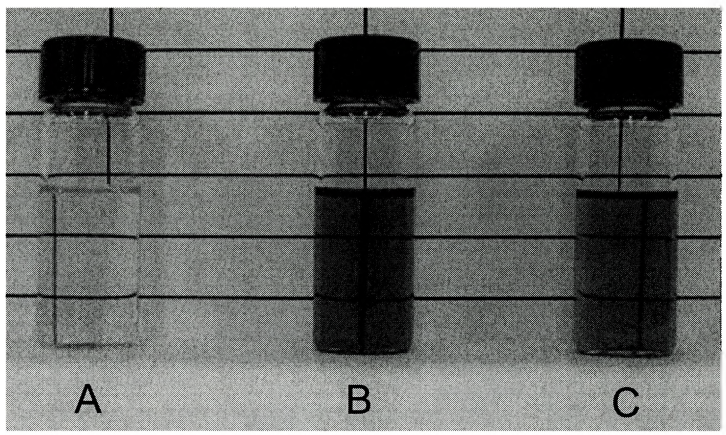

Figure 34. Photograph of (A) shortened SWNTs; (B) **16**; (C) **17** in $CHCl_3$.

These two composites were characterized by IR spectroscopy. To make a comparison, the IR spectrum of the unfunctionalized SWNTs is also shown in Figure 35A. The appearance of aliphatic C-H stretches (ca. 2900 cm^{-1}), and aromatic C-H stretches (ca. 3020 cm^{-1}) along with an aromatic C-C stretch at 1620 cm^{-1} in Figure 35B and C indicate the attachment of polymer chains after the radical coupling reaction. The strong absorbance at 1744 cm^{-1} is due to the C=O stretch arising from ester linkages in coumarin units. The similarity of the IR spectra of **16** and **17** confirms the resemblance of their structures.

The presence of nanotubes in these two composites was revealed by TEM analysis. The inset of Figure 36 shows a close-up view of a bundle of nanotubes spanning the gap between two areas of polymer.

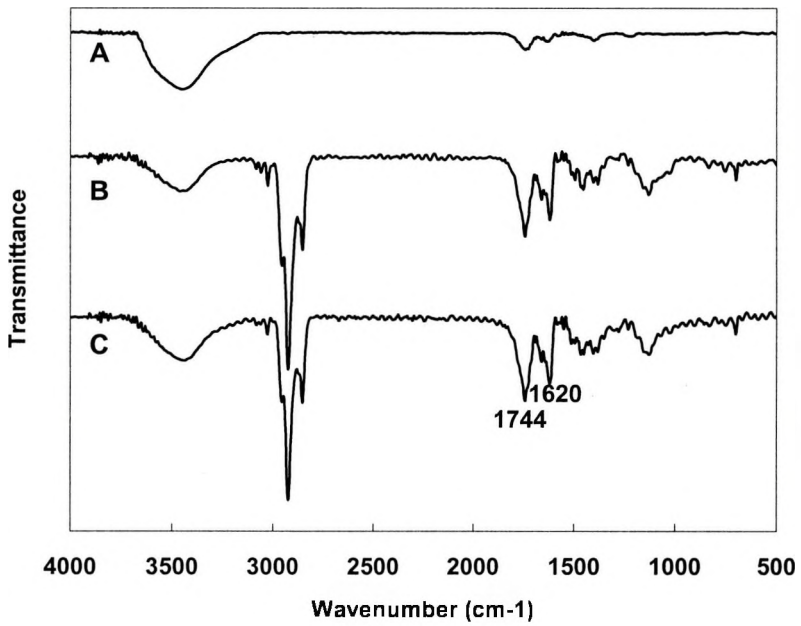

Figure 35. IR spectra for (A) the shortened, unfunctionalized SWNTs; (B) **16**; (C) **17**.

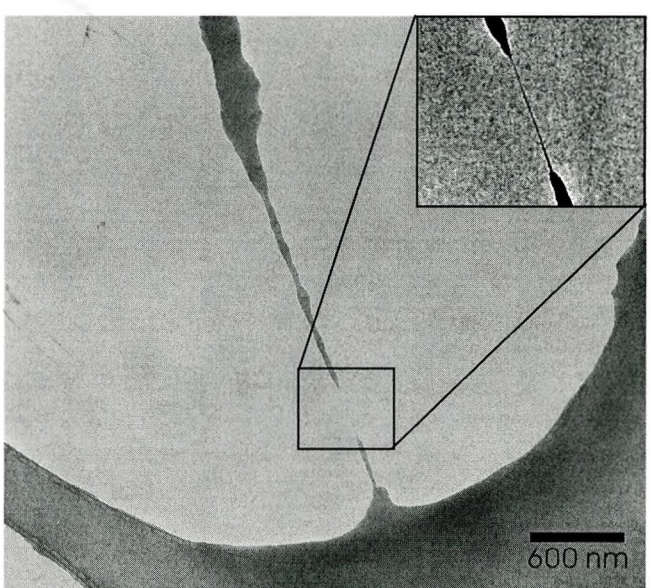

Figure 36. TEM micrograph of **16**. Inset shows a close-up view of a nanotube-bridged gap in the polymer structure.

Figure 37 illustrates the absorbance properties of these two composites in $CHCl_3$. Interestingly, a shoulder around 320 nm can be found in each case, although it is subtle. The difference between these two UV-Vis spectra and those of the coumarin-terminated PS functionalized SWNTs, where only one coumarin present on each PS chain, could be attributed to the increased concentration of coumarins relative to that of nanotubes in the composites **16** and **17**.

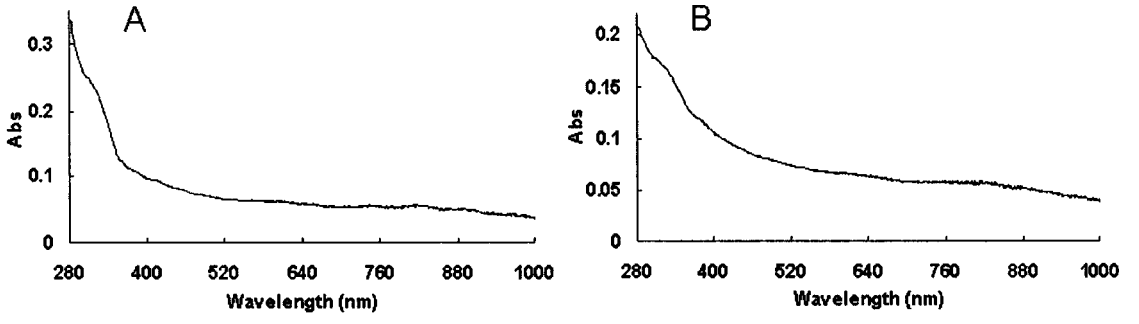

Figure 37. UV-Vis spectra of (A) **16**; (B) **17** in $CHCl_3$.

Figure 38 and Figure 39 illustrate the emission spectra of these two coumarin-containing copolymer functionalized SWNT composites and corresponding copolymers with excitation at 320 nm, all normalized at 391 nm. In both cases, the emission bands corresponding to coumarin-containing copolymers can still be observed for polymer functionalized SWNTs, and they were found to be broader than those of the starting copolymers. This suggests that the emission of these coumarins has not been quenched by the nanotubes, although some

chromophore-nanotube interactions, most likely π-π interactions, may be present in these composites, resulting in the observed optical broadening.

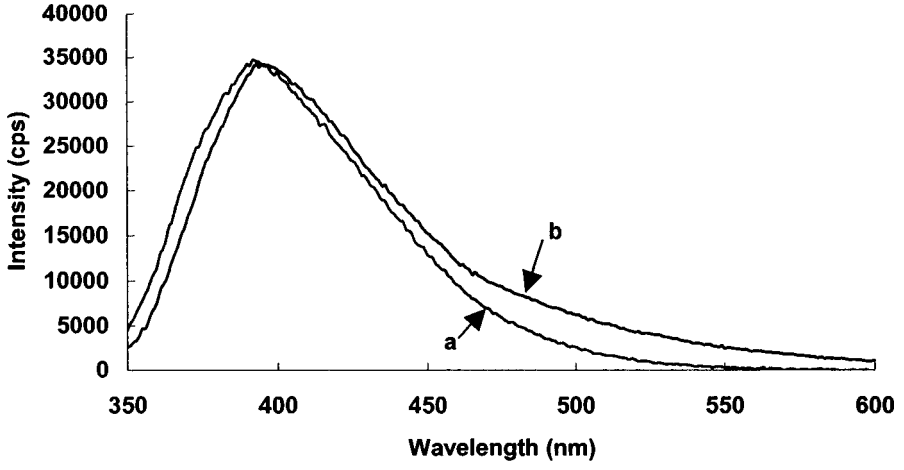

Figure 38. Overlay of normalized emission spectra for **14** in CH_2Cl_2 (λ_{em} 391 nm) (A), and **16** in $CHCl_3$ (λ_{em} 393 nm) (B).

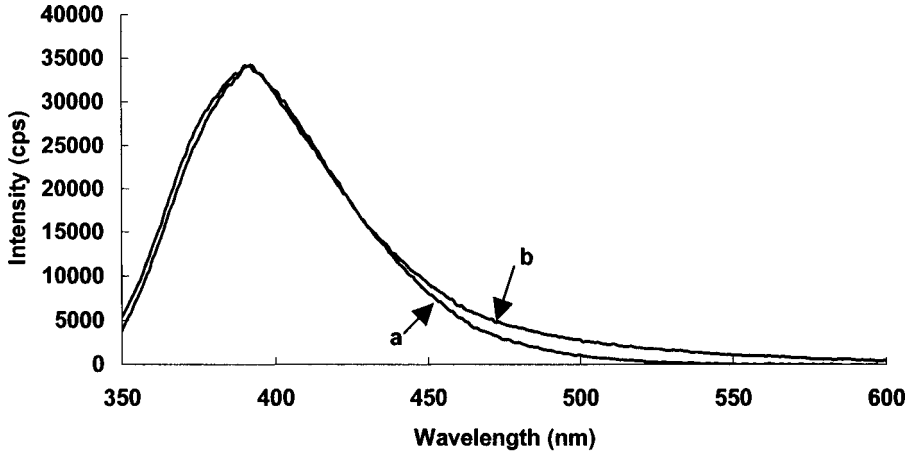

Figure 39. Overlay of normalized emission spectra for **15** in CH_2Cl_2 (λ_{em} 391 nm) (A), and **17** in $CHCl_3$ (λ_{em} 392 nm) (B).

3.5 Coumarin functionalized SWNTs

As a further extension of coumarin derivatives, we decided to explore the use of SFRP initiator **1** to prepare a third type of coumarin-containing compound, which could be used to put only one coumarin at a time directly on the surface of SWNTs in the hope of increasing the probability for photo-induced electrons being transferred to nanotubes.

3.5.1 Synthesis and characterization of coumarin attached alkoxyamine

Refluxing of a mixture of SFRP initiator **1**, 7-hydroxycoumarin, 18-crown-6, potassium carbonate, and potassium iodide in acetone for 6 hours led to the formation of coumarin attached alkoxyamine **18** in quantitative yield (Scheme 12). The reaction was monitored by TLC and the final product was purified by column chromatography using 7/3 Hexanes/EtOAc as the eluent. After drying in vacuum overnight, a white solid was obtained.

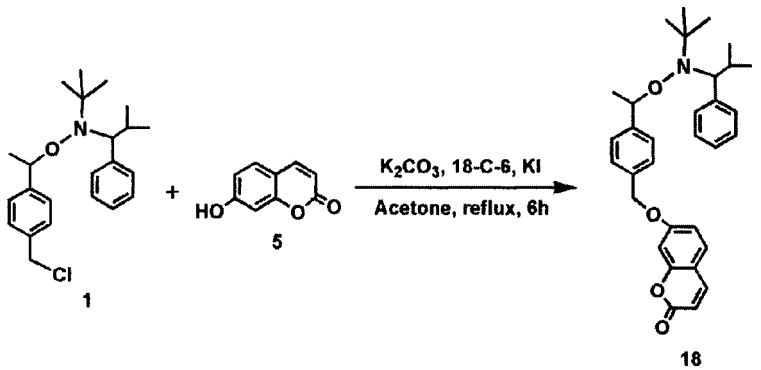

Scheme 12. Synthesis of coumarin attached alkoxyamine.

The product was fully characterized by Mass spectrometry and ^{1}H NMR as well as ^{13}C NMR. Mass spectrometry (Figure 40) gives a molecular weight of 500.3 Da (M+1), matching the expected molecular weight of **18**.

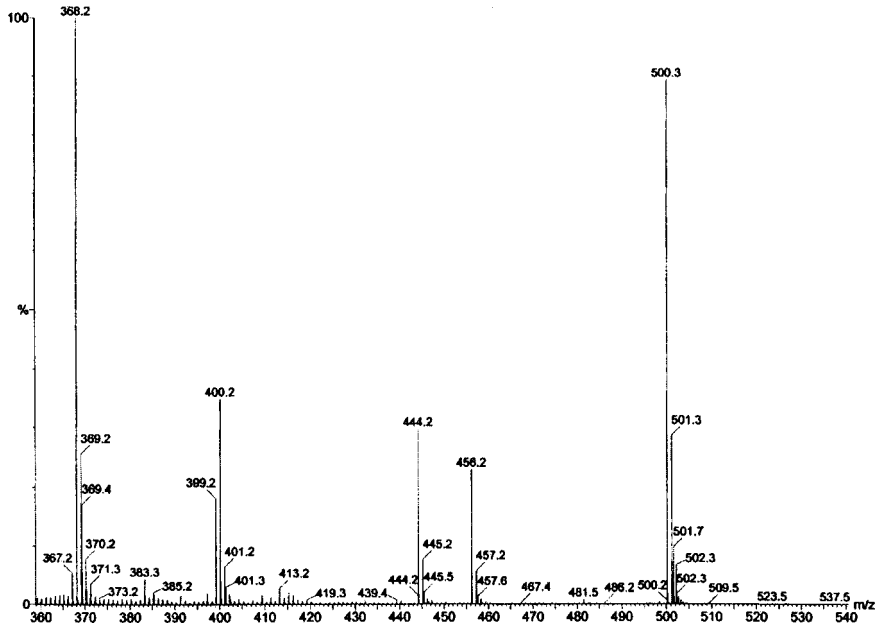

Figure 40. Mass spectrum of **18**.

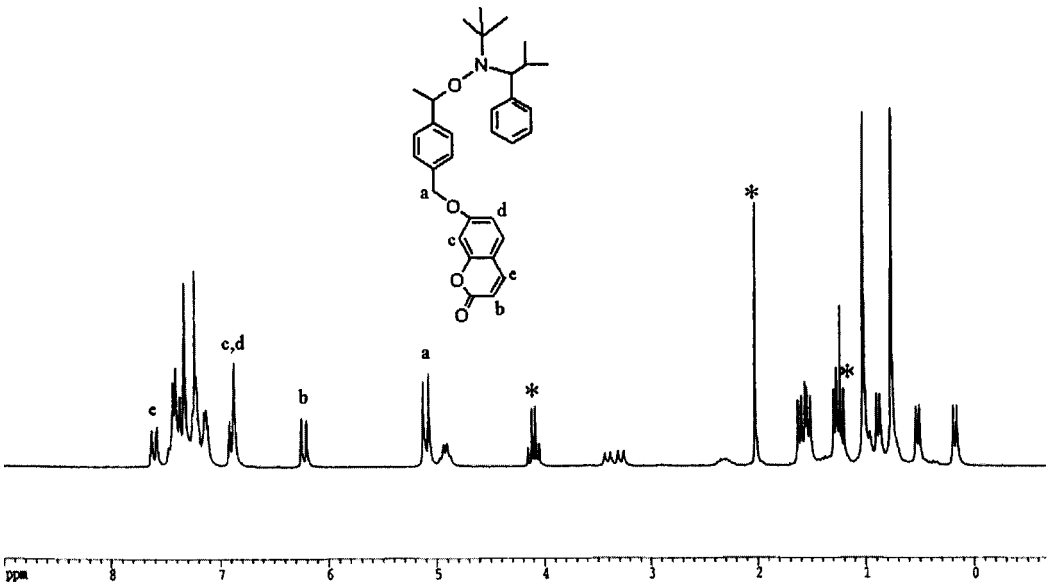

Figure 41. ^{1}H NMR spectrum of **18** in $CDCl_3$. (* ethyl acetate peaks)

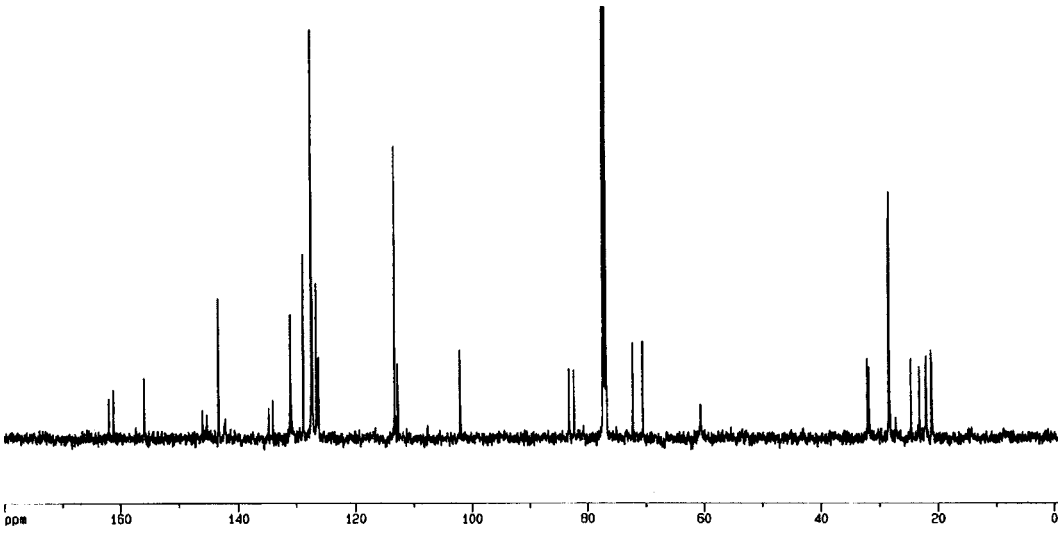

Figure 42. ^{13}C NMR spectrum of **18** in $CDCl_3$.

In Figure 41 (^1H NMR), the diagnostic signals for methylene protons next to ether linkage appear at 5.12 and 5.07 ppm due to the formation of diastereomers. Aromatic protons in the coumarin unit appear in the range of 6.20 to 7.64 ppm. The signals in ^{13}C NMR ranging from 101.1 to 161.1 ppm correspond to the sp^2 carbons of coumarin attached alkoxyamine **18** (Figure 42). The resonance at 161.9 ppm is characteristic for the C=O moiety. The signals at 70.5 ppm are diagnostic for the methylene carbon of the ether linkage. The signals for methyl carbons range from 21.0 to 28.4 ppm. All these characterizations indicate that the desired coumarin attached alkoxyamine has been synthesized.

3.5.2 Preparation and characterization of coumarin functionalized SWNTs

The preparation of coumarin attached alkoxyamine **18** functionalized SWNTs was accomplished by using the same procedure as that employed for coumarin containing polymer functionalized SWNTs outlined previously (Scheme 13).

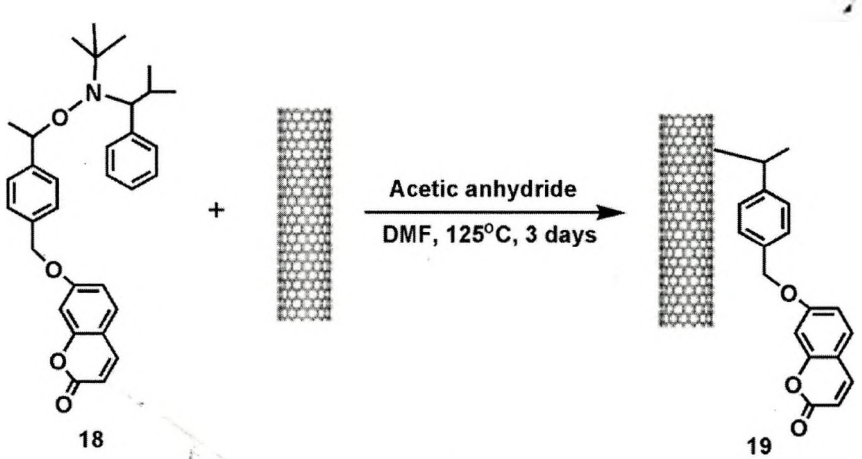

Scheme 13. Functionalization of SWNTs with coumarins.

This functionalization reaction was also followed by IR spectroscopy (Figure 43). The broad peaks ranging from 3010 to 2840 cm^{-1} correspond to the aliphatic C-H stretch and the aromatic C-H stretch from the attached coumarin derivative, and the appearance of a strong C=O stretch (ca. 1735 cm^{-1}) from the coumarin ester linkage is observable.

After functionalization, the resulting composites **19** were found to be insoluble in common organic solvents, such as THF, CH_2Cl_2, and $CHCl_3$. Again,

this demonstrates that the solubility of polymer functionalized SWNT composites discussed previously is due to the presence of polymers.

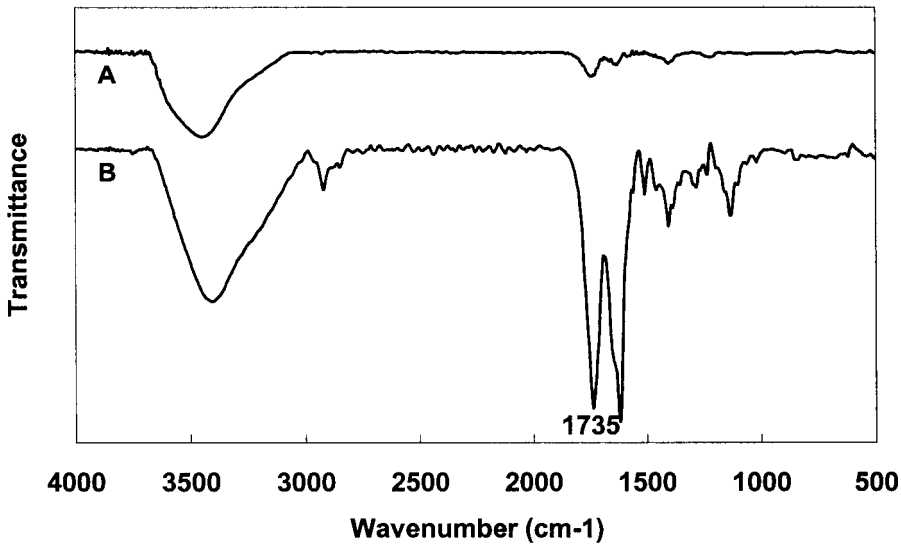

Figure 43. IR spectra for the shortened, unfunctionalized SWNT (A), and **19** (B).

3.5.3 Preparation and characterization of coumarin and PS functionalized SWNT composites

In order to make soluble nanotube composites with single coumarins sitting on the surface of SWNTs, "hetero" nanocomposites **20** were synthesized (Scheme 14). The addition of PS was aimed at the enhanced solubility of the resulting coumarin functionalized nanotube composite. Following the same process as that utilized for **19**, the coumarin and PS (M_n = 5246, PDI = 1.09) functionalized nanotube composites **20** was obtained by using a 1:1 molar ratio of **18** to PS.

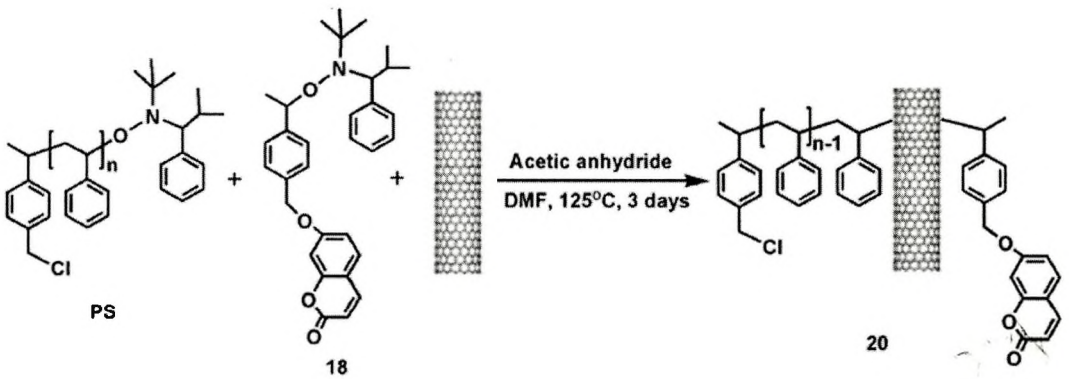

Scheme 14. Functionalization of SWNTs with PS and coumarins.

As expected, the resulting polymer functionalized coumarin-nanotube composite was found to be soluble in organic solvents, including CH_2Cl_2 and $CHCl_3$ (Figure 44).

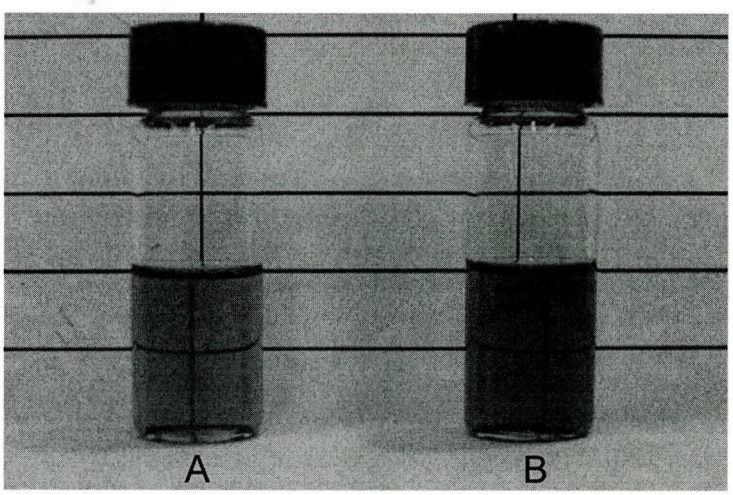

Figure 44. Solutions of **20** in CH_2Cl_2 (A), and $CHCl_3$ (B).

Figure 45 depicts the IR spectrum of the resulting PS and coumarin functionalized composite **20**. A strong stretch at 1717 cm^{-1} is due to the

attachment of coumarins, while strong stretches ca. 2900 cm^{-1} arise from the presence of polymers.

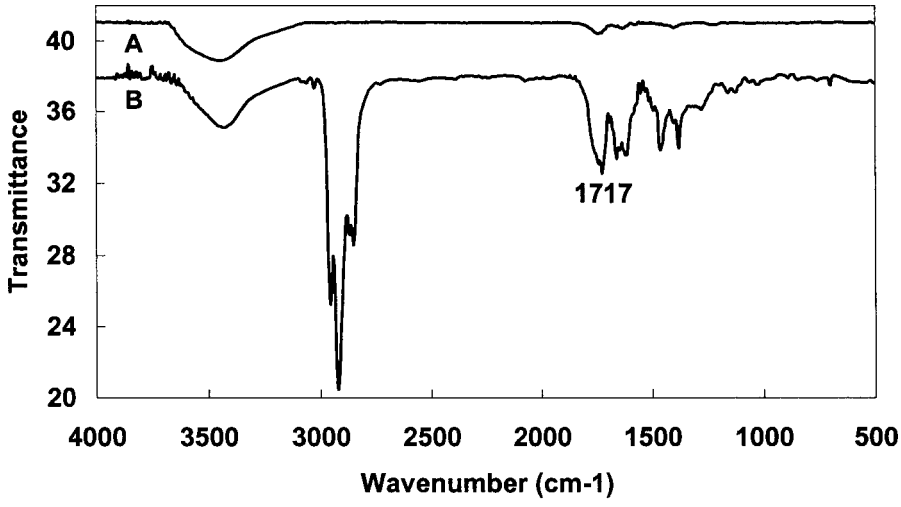

Figure 45. IR spectra for the shortened, unfunctionalized SWNT (A), and **20** (B).

The nanotube structures were analyzed by AFM and TEM. In Figure 46A, features with different heights along the nanotubes indicate that the nanotubes were not evenly functionalized. Similar to that of coumarin terminated PS functionalized SWNTs **10**, the TEM micrograph of **20** illustrates that individual nanotubes and small nanotube bundles are sheathed by regions of amorphous carbon (Figure 46B).

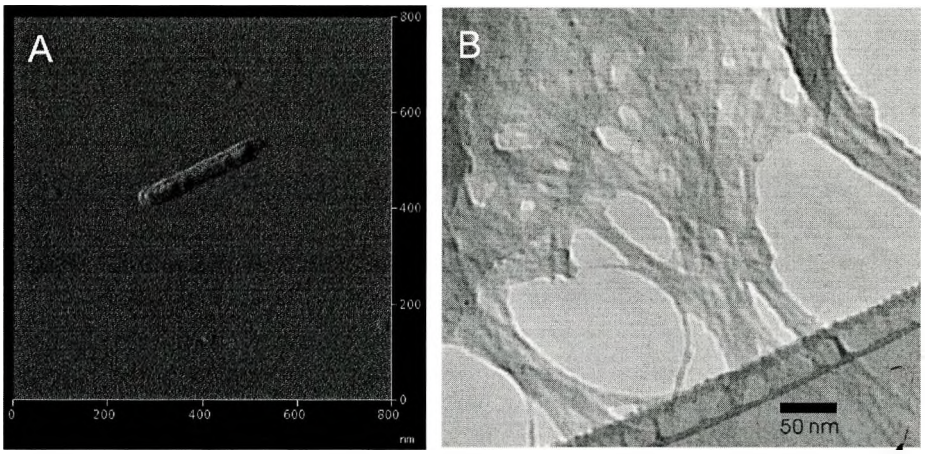

Figure 46. AFM image of **20** in CH_2Cl_2 (A), and TEM image of **20** (B).

Figure 47 illustrates the absorption properties of **20**. Unlike the spectra of copolymer functionalized SWNTs, where a distinct absorption at 320 nm characteristic for 7-hydroxycoumarin could be clearly seen, this spectrum is similar to those of coumarin terminated PS functionalized SWNTs. We believe that the relatively strong absorption arising from nanotubes overlaps the absorption of coumarins at 320 nm.

Figure 48 describes the emission spectra of the resulting composite **20** and coumarin attached alkoxyamine **18** with excitation at 320 nm, all normalized at the emission maximum. It is clear that the coumarin emission maximum is red-shifted upon attachment to the nanotube (shifts from 391 to 395 nm in **18** and **20**, respectively). Additionally, an extreme broadening can be observed in the spectrum of **20**. Considering the spectra for coumarin terminated PS functionalized SWNTs, and copolymer functionalized SWNTs, it can be

rationalized that the closer the coumarins are to the SWNTs, the stronger the chromophore-nanotube interactions become, resulting in broader emissions. The exact nature of this interaction and the reason for emission broadening are still unclear, and are the subject of ongoing investigation.

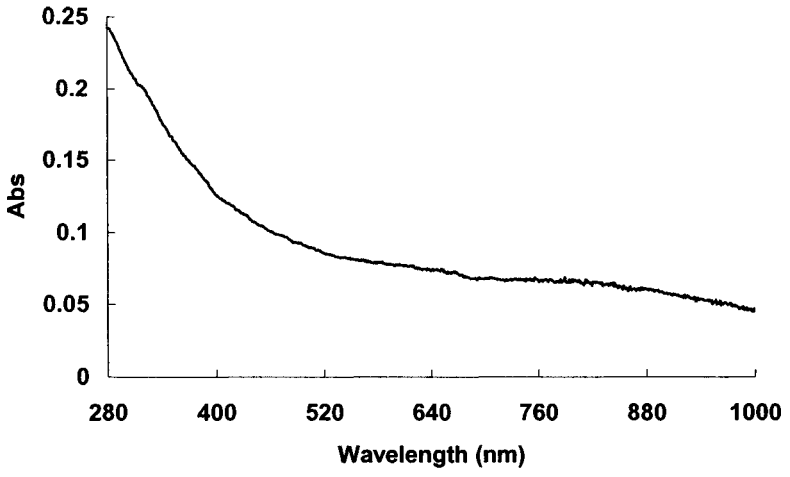

Figure 47. UV-Vis spectrum of **20** in $CHCl_3$.

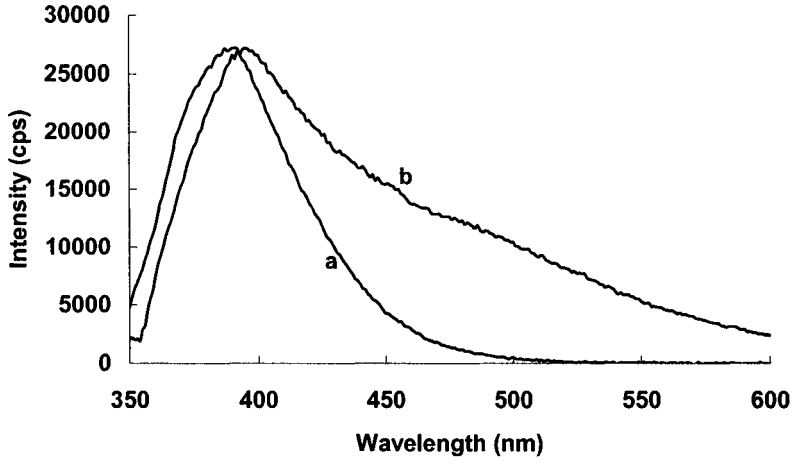

Figure 48. Overlay of normalized emission spectra for **18** in CH_2Cl_2 (λ_{em} 391 nm) (a), and **20** in $CHCl_3$ (λ_{em} 395 nm) (b).

3.6 Coumarin-343 terminated PS functionalized SWNTs

From the results shown so far, it is believed that chromophores with longer absorption wavelengths will help differentiate the absorption due to chromophores from that due to SWNTs since the absorption intensity of SWNTs decreases with increasing wavelength. This may possibly lead to a way to determine the quenching of the emissions of chromophores by SWNTs in a quantitative manner. To test this idea, coumarin-343 (λ_{max} 446 nm, λ_{em} 490 nm) terminated PS was chosen to perform the same analysis as 7-hydroxycoumarin terminated PS.

3.6.1 Preparation and characterization of Coumarin-343 functionalized PS

The same conditions as described previously were applied to synthesize coumarin-343 (C343) functionalized PS (PS-C343). The reaction of coumarin-343 **21** with PS (M_n = 4455, PDI = 1.07) in the presence potassium carbonate, 18-crown-6 in DMF for 1.5 hours led to the formation of coumarin-343 functionalized PS **22** (Scheme 15). The reaction was monitored by TLC and the product was purified by column chromatography using pure ethyl acetate as the eluent, followed by precipitation into methanol. After drying in a vacuum oven at 50°C overnight, a yellow powder was obtained (90% yield).

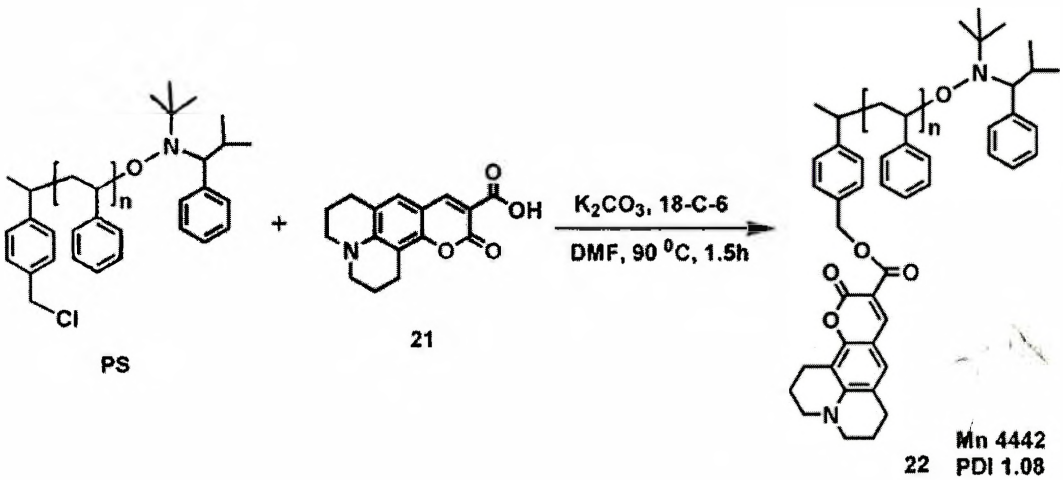

Scheme 15. Synthesis of Coumarin-343 terminated PS.

The complete conversion of the chloromethyl group at the PS chain end was confirmed by ^{1}H NMR. The signal at 4.52 ppm (Figure 49A), corresponding to the chloromethyl group of the starting material, completely disappeared after the reaction, and was replaced by a related signal at 5.26 ppm (Figure 49B). Other signals corresponding to C343 unit that are distinguishable from PS are also assignable as shown in Figure 49B. The attachment of C343 to PS was also confirmed by GPC, IR and ^{13}C NMR as in the case of 7-hydroxycoumarin terminated PS in section 3.3.1.

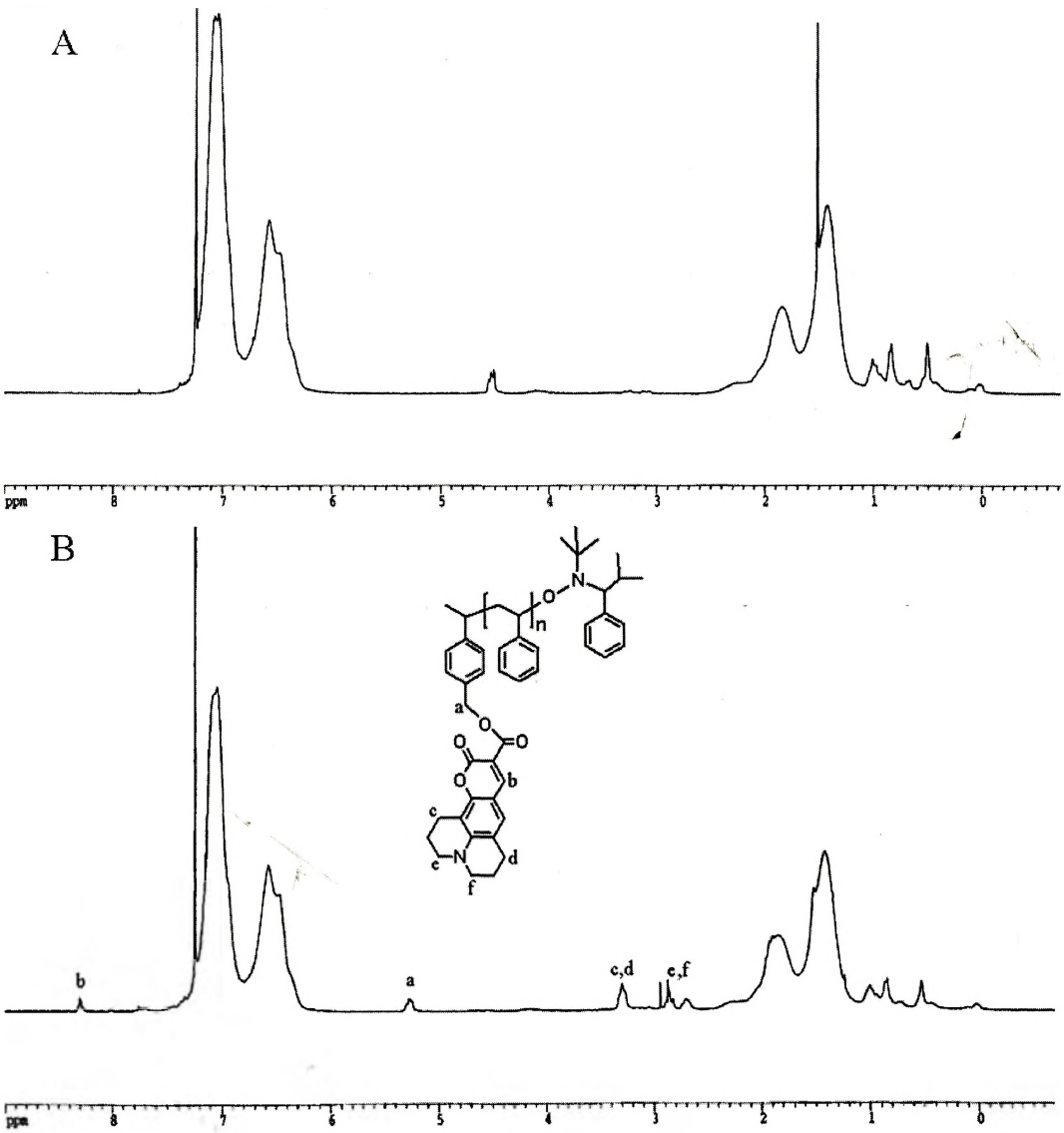

Figure 49. ^{1}H NMR spectra of PS (A), and **22** (B).

3.6.2 Preparation and characterization of SWNT-PS-C343 composites

Following the same method as that utilized for SWNT-PSOCoumarin, PS-C343 functionalized SWNT composites (SWNT-PS-C343) were obtained after

the reaction mixture was bubbled in DMF with N_2 for 30 min, and heated at 125 °C for 3 days (Scheme 16). The product **23** was purified by filtration through a 200 nm pore Teflon membrane, and washing with CH_2Cl_2, $CHCl_3$ and THF. TLC was used to ensure the complete removal of any unreacted small molecules and polymers. After drying in a vacuum oven at 50 °C overnight, a black residue was isolated, which doubled in mass over the shortened, unfunctionalized SWNTs.

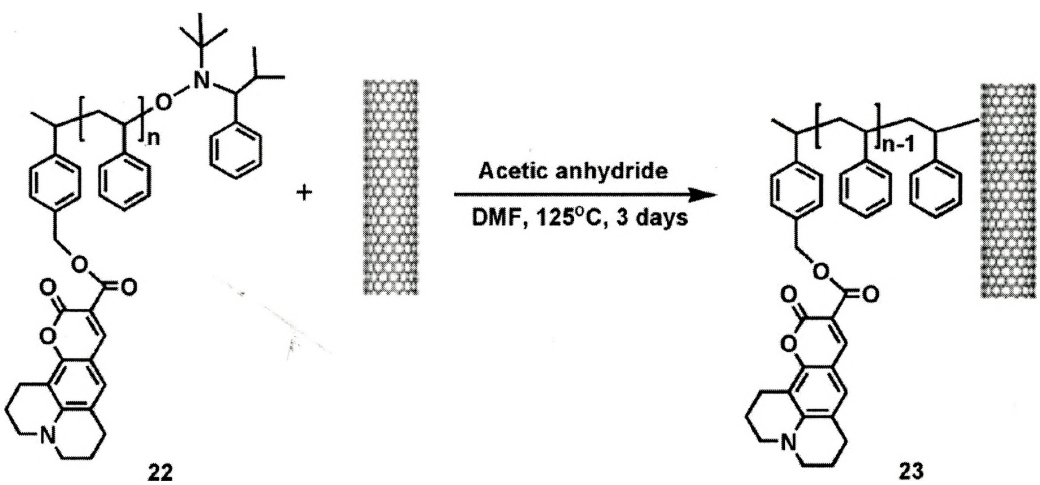

Scheme 16. Functionalization of SWNTs with PS-C343.

This functionalization reaction was again followed by IR spectroscopy to monitor the appearance of aliphatic C-H stretch (ca. 2900 cm^{-1}) and aromatic C-H stretches (3100 cm^{-1} to 3010 cm^{-1}) due to the attached polymer, and the appearance of a strong C=O stretch (1756 cm^{-1}) from the C343 ester group (Figure 50). It should be noted that the unreacted polymer recovered from this reaction was found to remain intact based on ^1H NMR and GPC analysis. This

means it is the attached C343 functionalized polymer that gives rise to the strong C=O stretch.

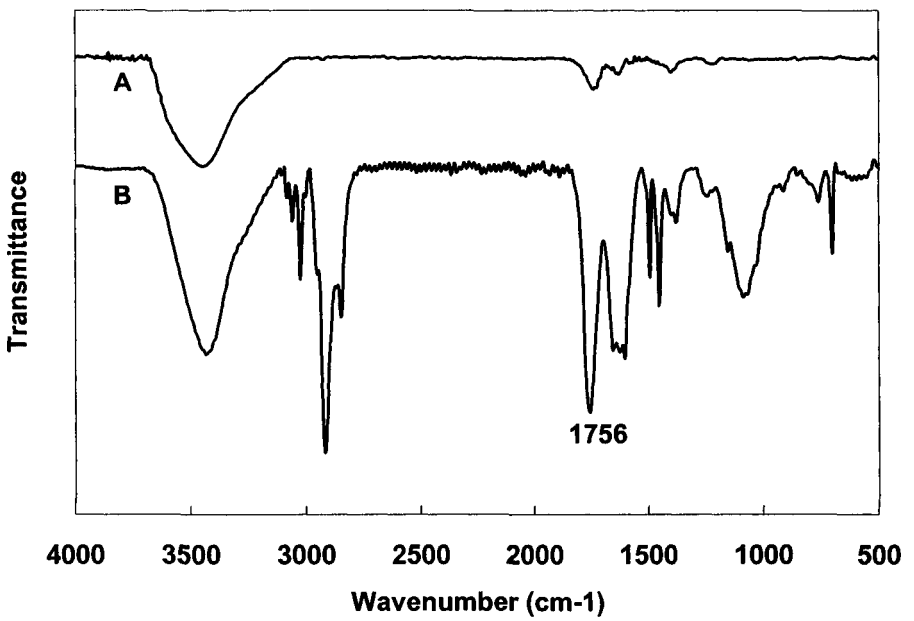

Figure 50. IR spectra for the shortened, unfunctionalized SWNT (A), and **23** (B).

The resulting composites **23** were found to be very soluble in CH_2Cl_2, THF and $CHCl_3$. Figure 51 shows the dark solutions of **23** in these solvents. In comparison, the shortened, unfunctionalized SWNTs settle down in these organic solvents making the liquid layer completely colorless as shown in section 3.2.2.

The direct evidence for the presence of carbon nanotubes in solutions can be determined from AFM analysis. Figure 52 presents the AFM images of **23** in different solvents. From these images, nanotubes can be easily observed. The uneven features along these composites indicate that the degree of the

functionalization of these nanotubes vary from nanotube to nanotube as well as from part to part in a same nanotube bundle. This is consistent with the AFM analysis shown previously.

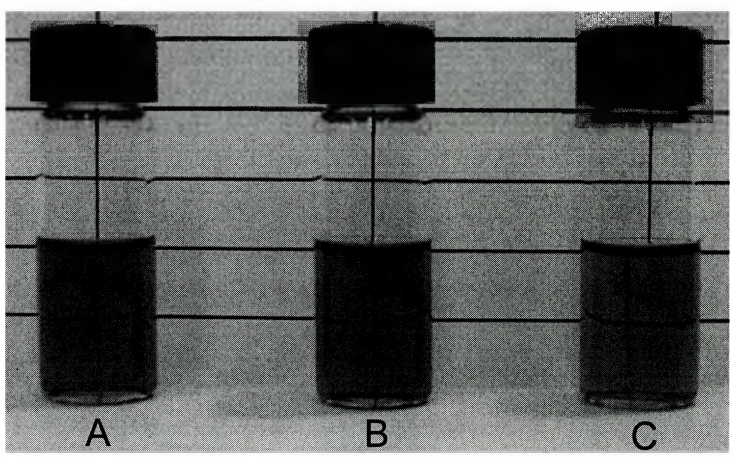

Figure 51. Solutions of **23** in (A) CH_2Cl_2; (B) $CHCl_3$; (C) THF.

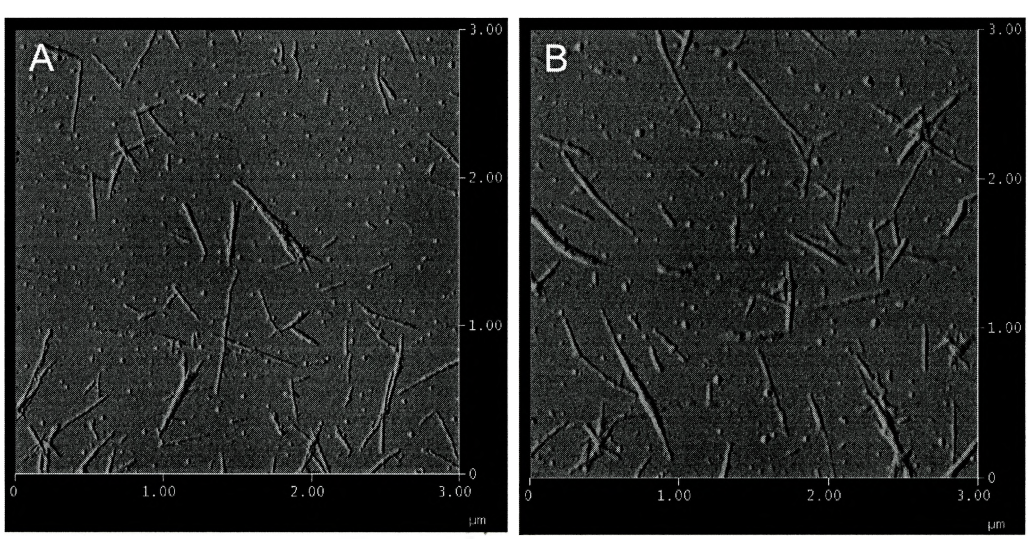

Figure 52. AFM images of **23** in $CHCl_3$ (A), and THF (B).

Figure 53 shows the UV-Vis spectrum of the resulting composite **23**. Although there is a peak around 440 nm, it is so small that it is hard to determine the relative intensity precisely by subtracting the absorption arising from nanotubes. In order to get a quantitative analysis of absorption spectra, chromophores with even longer absorption wavelengths that can be easily differentiated from the absorption of nanotubes are needed.

Figure 54 illustrates the emission spectra of the resulting composite **23** and coumarin-343 functionalized PS **22** with excitation at 437 nm, both normalized at the maximum of the emission band (467 nm). Again, the broadening of the resulting composite **23** was observed, which is believed to be due to the π-π interactions between the coumarins and nanotubes.

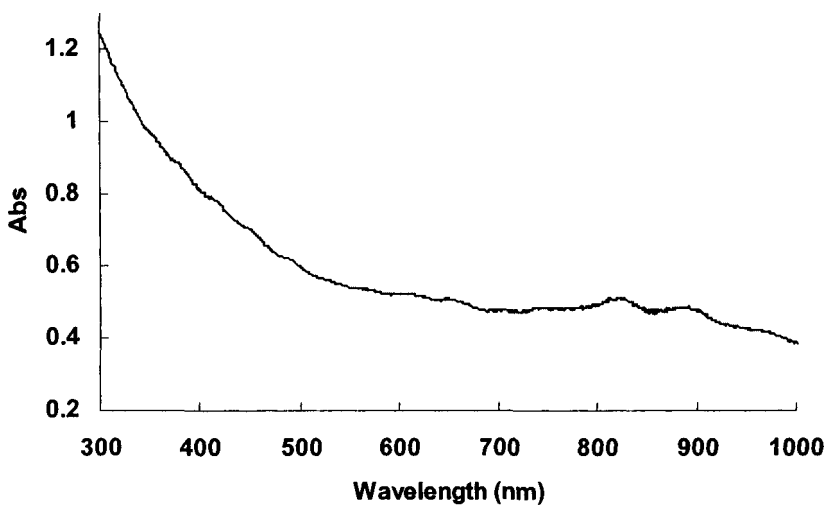

Figure 53. UV-Vis spectrum of **23** in CH_2Cl_2.

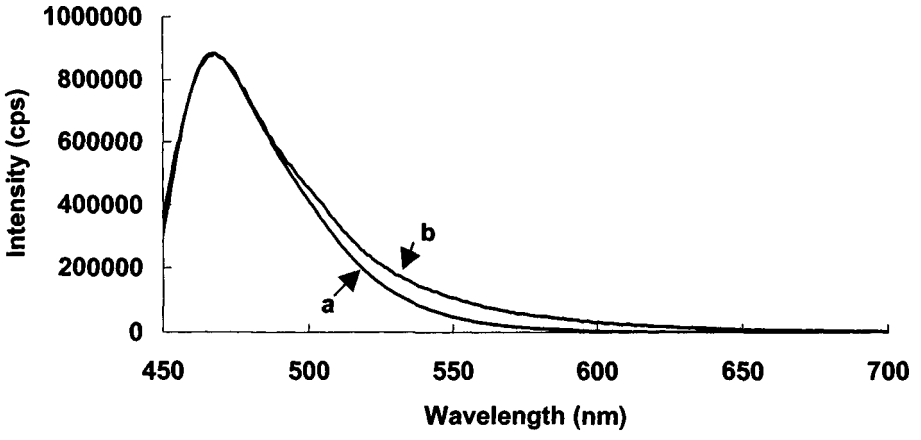

Figure 54. Overlay of normalized emission spectra for **22** (a), and **23** in CH_2Cl_2 (b).

Chapter 4 Conclusions

Novel coumarin-containing polymers with various structures made by derivatizing polystyrenes with coumarins or by SFRP using a synthetic chromophore-functionalized monomer were used in the functionalization of SWNTs via a one-pot radical coupling process. By utilizing this simple methodology, three categories of chromophore functionalized polymer nanotubes were successfully synthesized: coumarin-terminated PS functionalized SWNTs; coumarin-containing copolymer functionalized SWNTs; PS and coumarin hetero-functionalized SWNTs. IR and microscopy analysis including Atomic Force Microscopy (AFM) and Transmission Electron Microscopy (TEM) indicated that both polymers and nanotubes were present within these composites.

It was found that all these coumarin functionalized polymer nanotube composites were soluble in $CHCl_3$, which greatly improved the processibility of SWNTs. Consequently, it was possible to determine the absorption and emission properties of these composites by using UV-Vis and solution fluorescence measurements.

Different absorption behaviors have been observed for 7-hydroxycoumarin functionalized nanotube composites with different compositions. An attempt to

change the chromophore from 7-hydroxycoumarin (λ_{max} 325 nm) to coumarin-343 (λ_{max} 446 nm) did not lead to a clear differentiation for the absorption of coumarin-343 from that of nanotubes.

Fluorescence was still observed for all coumarin functionalized nanotube composites, and the π-π interactions between chromophores and nanotubes were believed to be responsible for the broadening of emission bands of the resulting composites. Unfortunately, quantitative fluorescence measurements to determine if any fluorescence quenching is occurring could not be performed because it was not possible to accurately determine the absorption intensity of the coumarins. This may require time-resolved fluorescence measurements in the future.

Overall, the one-pot synthesis of coumarin functionalized SWNTs via the radical coupling process provides a powerful tool to prepare potential soluble nanotube-based materials with better processibilities compared to insoluble nanotube chromophore blends.

Chapter 5 Experimental

General

Single-walled carbon nanotubes (SWNTs) were purchased from Carbon Nanotechnologies, Inc. (Houston, TX), purified and shortened by methods previously reported by our group. The nitroxide initiator, 2,2,5,5-tetramethyl-3-(1-phenylethoxy)-4-chloromethylphenyl-3-azahexane, compound **1** and the free nitroxide radical, 2,2,5,5-tetramethyl-4-phenyl-3-azahexane-3-nitroxide, compound **2** were prepared following the procedure reported by Hawker and coworkers. Styrene (Aldrich; 99%) was purified by filtration through basic alumina and stored in the refrigerator. All other reagents and solvents were purchased from commercial suppliers and used as received.

FTIR was measured on a FTS-40 instrument. All samples were prepared as pellets using spectroscopic grade KBr in a Carver press at 15,000 psi. Nuclear magnetic resonance (NMR) spectroscopy was performed on a Bruker 200 or 500 MHz NMR spectrometer using deuterated chloroform ($CDCl_3$) as solvent at room temperature.

Analytical thin-layer chromatography (TLC) was performed on commercial

Merck plates coated with silica gel GF254 (0.25 mm thick). Silica gel for flash chromatography was Merck Kieselgel 60 (230-400 mesh). Ultrasonication was done in a Banson Ultrasonics B1510 bath sonicator. Filtration was done through either a 100 nm-pore polycarbonate membrane (Millipore) or a 200 nm-pore Teflon membrane (Millipore).

Polymer molecular weight and polydispersity index (PDI) were estimated by gel permeation chromatography (GPC) using a Waters 2695 Separations Module connected to a Waters 2414 Refractive Index Detector, Waters 2996 Photodiode Array Detector, and Waters 2475 Multi λ Fluorescence Detector with tetrahydrofuran (THF) as the mobile phase at a flow rate of 1.0 mL/min. Molecular weight standards used for calibration of the GPC system were narrow polydispersity polystyrene. All samples were run in THF at 35°C. The fluorescence detector was set to an emission wavelength of 390 nm, and an excitation wavelength of 325 nm for 7-hydroxycoumarin derivatives, and an emission wavelength of 435 nm, and an excitation wavelength of 490 nm for coumarin 343 derivatives.

Atomic force microscopy (AFM) experiments were carried out in air with a Digital Instruments NanoScope IIIa Multimode system operated with standard silicon tips in tapping mode at a scan rate of 1 Hz. The samples were prepared for

AFM analysis by spincoating sample solutions or suspensions onto freshly cleaved mica substrates. TEM was recorded on a Philips CM12 instrument operating at 120 keV. UV absorption measurements were performed on a Varian Cary 50 Bio UV-Visible Spectrophotometer, and fluorescence emission spectra were recorded on a SPEX Fluorolog 3-22 Fluorimeter.

Shortening and Purification of SWNTs

A 500 mL flask charged with 100 mg of SWNTs and 110 mL of a H_2SO_4/HNO_3 (v/v: 80/30) solution was sonicated for 2 hours. The mixture was then transferred to a 1 L beaker, and diluted with 800 mL of distilled water. After cooling to room temperature, the diluted solution was filtered through a 100 nm-pore polycarbonate membrane. The black material collected from the membrane was further treated by stirring with 50 mL of H_2SO_4/H_2O_2 (9/1) in a 250 mL flask for 30 min at room temperature. Another 50 mL of H_2SO_4/H_2O_2 (9/1) was added and the solution was sonicated for 5 min. After dilution using 500 mL of distilled water, the solution was filtered through a 100 nm-pore polycarbonate membrane. The resulting mat of SWNTs was washed thoroughly using first distilled water, then a 5 mM NaOH solution, and then distilled water until the pH of the filtrate was 7. The purified SWNTs were then dried in vacuum overnight.

IR (KBr pellet): 1741, 1627 cm^{-1}.

General procedure for the formation of PS by SFRP; PS (3)

Mixtures of styrene, the nitroxide initiator **1**, acetic anhydride and chlorobenzene were added to a round-bottom flask, degassed by bubbling with nitrogen for 30 minutes, and sealed with a rubber septum under argon. The feed ratios of initiator **1**: acetic anhydride was approximately 1: 0.05. In a typical experiment, a round-bottom flask equipped with a magnetic stir bar was charged with styrene (3.0 g, 28.8 mmol), initiator, **1** (114.9 mg, 0.31 mmol), acetic anhydride (35.6 mg, 0.35 mmol), chlorobenzene (3 mL), and was sealed with a rubber septum. After bubbling with nitrogen for thirty minutes, the deoxygenated solution was stirred at 125°C under argon in a temperature-controlled oil bath for 20 h. The resulting polystyrene was dissolved in 3 mL of CH_2Cl_2 and drop-wise precipitated into 300 mL of methanol. The precipitate was then collected by vacuum filtration and dried to give the desired polystyrene, **3**, as a white solid (2.732 g, 88% yield), M_n = 9693, PDI = 1.08. ^1H NMR (200 MHz, $CDCl_3$): δ 7.05 (broad), 6.56 (broad), 4.52 (s, 2H), 1.84 (broad), 1.42 (broad), 0.99 (broad), 0.83 (broad), and 0.50 (broad). ^{13}C NMR (500 MHz, $CDCl_3$): δ 27.8, 40.7, 44.2, 44.3, 44.4, 44.5, 44.7, 125.7, 125.9, 127.7, 127.9, 128.2, 145.5, 145.6, 145.9, and 146.3.

General procedure for the formation of polymer functionalized SWNTs via radical coupling reactions; Polystyrene functionalized SWNTs (SWNT-PS) (4)

To a suspension of purified SWNTs (9.6 mg) in DMF (10 mL) in a 50 mL flask were added acetic anhydride (0.05 mL, 0.53 mmol) and polystyrene **3** (Mn = 9693 g/mol, 500 mg). The mixture was degassed by bubbling with N_2 for 30 min and was then stirred at 125°C under argon for 3 days. The product polymer-functionalized SWNTs were purified by washing extensively with CH_2Cl_2, $CHCl_3$ and THF during filtration through a 200 nm-pore Teflon membrane. Drying under vacuum overnight gave **4** as a black solid. The mass increased by approximately 100%. ^{1}H NMR (200MHz, $CDCl_3$): δ 7.06 (broad), 6.56 (broad), 1.83 (broad) and 1.43 (broad). IR (KBr pellet): 3087-3025, 2960-2836, 1605, 1495, 1451 cm^{-1}.

General procedure for the formation of coumarin terminated polystyrenes; 7-Hydroxcoumarin terminated PS (6)

The mixture of 7-Hydroxycoumarin **5** (70.5 mg, 0.44 mmol), potassium carbonate (96.6 mg, 0.70 mmol) and 18-Crown-6 (31.6 mg, 0.12 mmol) and a catalytic amount of KI in 8 mL of DMF was stirred at 90 °C under argon for 30

min. PS (M_n=2416, PDI=1.07, 713.3 mg, 0.30 mmol) was then added. The reaction mixture was stirred at 90 °C under argon for another 4 hours. It was then cooled, evaporated to dryness, taken up in EtOAc, filtered, concentrated, and purified by chromatography on silica gel using 5/5 EtOAc/Hexanes as the eluent. The precipitation of the colorless oil from chromatography into methanol gave 604.6 mg of **6** as a white powder (81%). ^{1}H NMR (200 MHz, $CDCl_3$): δ 7.07 (broad), 6.57 (broad), 5.01 (s, 2H), 1.83 (broad), 1.43 (broad), 0.99 (broad), 0.84 (broad), and 0.53 (broad).

7-Hydroxcoumarin terminated PS (7)

7-Hydroxycoumarin terminated PS, **7**, was prepared from PS (M_n=4572, PDI=1.07) using the general procedure as described above. The ratio of **5**/K_2CO_3/18-C-6/PS was 45.0 mg (0.28 mmol)/61.0 mg (0.44 mmol)/18.9 mg (0.071 mmol)/1.0001 g (0.21 mmol). Yield: 857.5 mg (84%). ^{1}H NMR (200 MHz, $CDCl_3$): δ 7.07 (broad), 6.58 (broad), 5.01 (s, 2H), 1.82 (broad), and 1.41 (broad), and 0.99 (broad)).

7-Hydroxcoumarin terminated PS (8)

7-Hydroxycoumarin terminated PS, **8**, was prepared from PS (M_n=8380,

PDI=1.10) using the general procedure as described above. The ratio of **5**/K_2CO_3/18-C-6/PS was 26.5 mg (0.16 mmol)/36.2 mg (0.26 mmol)/12.8 mg (0.048 mmol)/1.089 g (0.13 mmol). Yield: 965.7 mg (87%). ^{1}H NMR (200 MHz, $CDCl_3$): δ 7.04 (broad), 6.57 (broad), 5.01 (s, 2H), 1.82 (broad), and 1.41 (broad), and 0.99 (broad).

7-Hydroxcoumarin terminated PS functionalized SWNTs (9)

The polymer functionalized composite, **9**, was prepared from 7-hydroxcoumarin terminated PS, **6**, using the general polymer nanotube coupling procedure described above. The ratio of SWNTs/**5**/acetic anhydride was 7.8 mg/380 mg/0.04 mL (43.2 mg). Purification by filtration through a 200 nm-pore Teflon membrane and washing with CH_2Cl_2, $CHCl_3$ and THF, afforded **9** as a black solid, 10.0 mg. IR (KBr pellet): 3090-3020, 2960-2836, 1722, 1645, 1495, 1452 cm^{-1}.

7-Hydroxcoumarin terminated PS functionalized SWNTs (10)

The polymer functionalized composite, **10**, was prepared from 7-hydroxcoumarin terminated PS, **7**, using the general polymer nanotube coupling procedure described above. The ratio of SWNTs/**7**/acetic anhydride was 7.8

mg/380 mg/0.04 mL (43.2 mg). Purification by filtration through a 200 nm-pore Teflon membrane and washing with CH_2Cl_2, $CHCl_3$ and THF, afforded **10** as a black solid, 10.4 mg. IR (KBr pellet): 3090-3020, 2962-2840, 1723, 1646, 1495, 1459 cm^{-1}.

7-Hydroxcoumarin terminated PS functionalized SWNTs (11)

The polymer functionalized composite, **11**, was prepared from 7-hydroxcoumarin terminated PS, **8**, using the general polymer nanotube coupling procedure described above. The ratio of SWNTs/**7**/acetic anhydride was 8.0 mg/400 mg/0.04 mL (43.2 mg). Purification by filtration through a 200 nm-pore Teflon membrane and washing with CH_2Cl_2, $CHCl_3$ and THF, afforded **11** as a black solid, 9.7 mg. IR (KBr pellet): 3070-3020, 2960-2840, 1722, 1649, 1494, 1461 cm^{-1}.

7-styrylmethoxycoumarin (13)

The mixture of 7-Hydroxycoumarin **5** (974.4 mg, 6.01 mmol), potassium carbonate (2.4904 g, 18.05 mmol) and 18-Crown-6 (31.6 mg, 1.14 mmol) and a catalytic amount of KI in 65 mL of acetone was stirred at reflux under argon for 30 min. VBC, **12** (0.93 mL, 6.59 mmol), was then added. The reaction mixture

was stirred at reflux for another 4.5 hours. It was then cooled, evaporated to dryness, taken up in CH_2Cl_2, filtered, concentrated, and purified by chromatography on silica gel using CH_2Cl_2 as the eluent to yield 1.5146 g of **13** as a colorless viscous oil that solidified on standing (91%). ^{1}H NMR (200 MHz, $CDCl_3$): δ 7.60 (d, J = 9.5 Hz, 1H), 7.43-7.34 (m, 5H), 6.90-6.86 (m, 2H), 6.70 (dd, J = 10.9 Hz, 17.6 Hz, 1H), 6.22 (d, J = 9.5 Hz, 1H), 5.74 (d, J = 17.6 Hz, 1H), 5.25 (d, J = 10.9 Hz, 1H), 5.09 (s, 2H). ^{13}C NMR (500 MHz, $CDCl_3$): 161.85, 161.05, 155.84, 143.26, 137.79, 136.28, 135.24, 128.76, 127.73, 126.56, 114.43, 113.28, 113.21, 112.76, 101.99, 70.30. M.S. (E. I.): Calcd m/z = 278.1. Found m/z = 278.1 [M^+].

Poly[styrene-*b*-(7-styrylmethoxycoumarin)] (14)

The nitroxide terminated PS (M_n = 5449, PDI = 1.12, 654.3 mg, 0.12 mmol), monomer **13** (335.3 mg, 1.20 mmol), acetic anhydride (73.5 mg, 0.72 mmol) and free nitroxide **2** (2.6 mg, 0.012 mmol), were dissolved in 9 mL of DMF in a 50 mL round bottom flask, degassed by bubbling with nitrogen for 30 minutes, and sealed with a rubber septum under argon. The polymerization was carried out in an oil bath regulated at 125°C under argon for 1 hour. The reaction mixture was then precipitated into 100 mL of methanol. The precipitate was then collected by

vacuum filtration, taken up in EtOAc, and purified by column chromatography, eluting with 5/5 Hexanes/EtOAc, followed by pure EtOAc. The precipitation of the colorless oil from chromatography into methanol gave 115.6 mg of **14** as a white powder, M_n = 8493 g/mol, PDI = 1.15. ^{1}H NMR (200 MHz, $CDCl_3$): δ 7.55 (broad), 7.31 (broad), 7.07 (broad), 6.21 (broad), 4.92 (broad), 4.52 (broad), 1.81 (broad), 1.43 (broad), and 0.99 (broad).

Poly[styrene-*r*-(7-styrylmethoxycoumarin)] (15)

A round-bottom flask equipped with a magnetic stir bar was charged with styrene (0.34 mL, 3.0 mmol), monomer, **13** (139 mg, 0.5 mmol), initiator, **1** (33.7 mg, 0.09 mmol), free nitroxide **2** (0.99 mg, 4.5×10^{-3} mmol), acetic anhydride (23.8 mg, 0.23 mmol), DMF (1 mL), and was sealed with a rubber septum. After bubbling with nitrogen for thirty minutes, the deoxygenated solution was stirred at 125°C under argon in a temperature-controlled oil bath for 20 h. The resulting polymer was dissolved in 1 mL of CH_2Cl_2 and drop-wise precipitated into 50 mL of methanol. Reprecipitation using the same procedure gave the random copolymer, **15**, as a white powder (174.6 mg), M_n = 4254 g/mol, PDI = 1.33. ^{1}H NMR (200 MHz, $CDCl_3$): δ 7.57 (broad), 7.31 (broad), 7.07 (broad), 6.23 (broad), 4.96 (broad), 4.52 (broad), 1.80 (broad), 1.41 (broad), and 0.98 (broad).

Poly[styrene-*b*-(7-styrylmethoxycoumarin)] functionalized SWNTs (16)

The block copolymer functionalized composite, 15, was prepared from poly[styrene-*b*-(7-styrylmethoxycoumarin)], **14**, using the general polymer nanotube coupling procedure described above. The ratio of SWNTs/**14**/acetic anhydride was 4.7 mg/97.0 mg/0.035 mL (37.8 mg). Purification by filtration through a 200 nm-pore Teflon membrane and washing with CH_2Cl_2, $CHCl_3$ and THF, afforded **16** as a black solid, 6.2 mg. IR (KBr pellet): 3070-3020, 2960-2840, 1742, 1619, 1495, 1455 cm^{-1}.

Poly[styrene-*r*-(7-styrylmethoxycoumarin)] functionalized SWNTs (17)

The random copolymer functionalized composite, **17**, was prepared from poly[styrene-*r*-(7-styrylmethoxycoumarin)], **15**, using the general polymer nanotube coupling procedure described above. The ratio of SWNTs/**15**/acetic anhydride was 4.2 mg/150 mg/0.03 mL (32.4 mg). Purification by filtration through a 200 nm-pore Teflon membrane and washing with CH_2Cl_2, $CHCl_3$ and THF, afforded **17** as a black solid, 6.8 mg. IR (KBr pellet): 3070-3020, 2960-2840, 1742, 1620, 1494, 1453 cm^{-1}.

Coumarin attached alkoxyamine (18)

The mixture of 7-Hydroxycoumarin **5** (243.8 mg, 1.50 mmol), potassium carbonate (497.1 mg, 3.6 mmol) and 18-Crown-6 (65.0 mg, 0.25 mmol) and a catalytic amount of KI in 8 mL of acetone was stirred at reflux under argon for 30 min. 2,2,5,5-tetramethyl-3-(1-phenylethoxy)-4-chloromethylphenyl-3-azahexane, **1** (448.8 mg, 1.20 mmol), was then added. The reaction mixture was stirred at reflux for another 6 hours. It was then cooled, evaporated to dryness, taken up in EtOAc, filtered, concentrated, and purified by chromatography on silica gel using 7/3 Hexanes/EtOAc as the eluent to afford **18** as a colorless viscous oil that solidified on standing (quantitative yield). ^{1}H NMR (200 MHz, $CDCl_3$, both diastereomers): δ 7.61 (d, J = 9.5 Hz, 2H), 7.44-7.12 (m, 20H), 6.91-6.87 (m, 4H), 6.23 (d, J = 9.5 Hz, 2H), 5.12 (s, 2H), 5.07 (s, 2H), 4.91 (m, 2H), 3.40 (m, 1H), 3.29 (m, 1H), 2.30 (m, 2H), 1.60 (m, 3H), 1.52 (m, 3H), 1.25 (m, 3H), 1.02 (s, 9H), 0.87 (m, 3H), 0.74 (s, 9H), 0.52 (d, J = 6.6 Hz, 3H), 0.18 (d, J = 6.6 Hz, 3H). ^{13}C NMR (500 MHz, $CDCl_3$): 161.96, 161.08, 155.86, 146.03, 145.28, 143.29, 134.71, 134.03, 130.95, 128.74, 127.32, 127.20, 126.56, 126.38, 126.21, 113.23, 112.72, 102.0, 83.19, 82.32, 72.22, 70.48, 60.57, 32.01, 31.72, 28.39, 28.24, 24.63, 23.14, 22.07, 21.93, 21.00. M.S. (C. I.): Calcd m/z = 499.6. Found m/z =500.3 (M+1).

7-Hydroxycoumarin functionalized SWNTs (19)

The coumarin functionalized composite, **19**, was prepared from coumarin-attached alkoxyamine, **18**, using the same method as those used for polymer-nanotube composites. The ratio of SWNTs/**18**/acetic anhydride was 7.4 mg/200.2 mg/0.04 mL (43.2 mg). Purification by filtration through a 200 nm-pore Teflon membrane and washing with CH_2Cl_2, $CHCl_3$ and THF, afforded **19** as a black solid, 7.6 mg. IR (KBr pellet): 3010-2840, 1735, 1618, 1507, 1457, 1385 cm^{-1}.

PS and 7-hydroxycoumarin functionalized SWNTs (20)

The PS and coumarin functionalized composite, **20**, was prepared from PS (M_n = 5246, PDI = 1.09) and coumarin attached alkoxyamine, **18**, using the general polymer nanotube coupling procedure described above. The ratio of SWNTs/PS/**18**/acetic anhydride was 8.1 mg/411.2 mg/39.5 mg/0.04 mL (43.2 mg). Purification by filtration through a 200 nm-pore Teflon membrane and washing with CH_2Cl_2, $CHCl_3$ and THF, afforded **20** as a black solid, 10.0 mg. IR (KBr pellet): 3083, 3024, 2980-2840, 1717, 1660, 1620, 1497, 1462, 1379 cm^{-1}.

Coumarin-343 terminated PS (22)

Coumarin-343 terminated PS, **22**, was prepared from PS (M_n = 4455, PDI = 1.07) using the same methods as those used for 7-hydroxycoumarin terminated PS. The ratio of **21**/K_2CO_3/18-C-6/PS was 40 mg (0.14 mmol)/31 mg (0.22 mmol)/5 mg (0.019 mmol)/500 mg (0.11 mmol). Specifically, the reaction mixture in 4 mL of DMF was stirred at 90 °C under argon for 1.5 hours. Purification by column chromatography using EtOAc as the eluent, followed by precipitation into methanol, gave 474 mg of the desired polymer, **22**, as a yellow solid (90% yield), M_n = 4442 g/mol, PDI = 1.08. ^{1}H NMR (200 MHz, $CDCl_3$): δ 8.30 (broad), 7.07 (broad), 6.57 (broad), 5.26 (broad), 3.30 (broad), 2.85 (broad), 2.68 (broad), 1.86 (broad), and 1.42 (broad), 1.00 (broad), 0.85 (broad), and 0.53 (broad).

Coumarin-343 terminated PS functionalized SWNTs (23)

The polymer functionalized composite, **23**, was prepared from coumarin-343 terminated PS, **22**, using the general polymer nanotube coupling procedure. The ratio of SWNTs/**22**/acetic anhydride was 4.8 mg/210 mg/0.03 mL (32.4 mg). Purification by filtration through a 200 nm-pore Teflon membrane and washing with CH_2Cl_2, $CHCl_3$ and THF, afforded **23** as a black solid, 9.5 mg. IR (KBr pellet): 3090-3000, 2960-2810, 1759, 1599, 1491, 1454 cm^{-1}.

References:

(1) Iijima, S. *Nature* **1991**, *354*, 56-58.

(2) Iijima, S.; Ichihashi, T. *Nature* **1993**, *363*, 603-605.

(3) Sloan, J.; Wright, D. M.; Woo, H. G.; Bailey, S.; Brown, G.; York, A. P. E.; Coleman, K. S.; Hutchison, J. L.; Green, M. L. H. *Chem. Commun.* **1999**, 699-700.

(4) Ajayan, P. M.; Lambert, J. M.; Bernier, P.; Barbedette, L.; Colliex, C.; Planeix, J. M. *Chem. Phys. Let.t* **1993**, *215*, 509-517.

(5) Guo, T.; Nikolaev, P.; Thess, A.; Colbert, D. T.; Smalley, R. E. *Chem. Phys. Lett.* **1995**, *243*, 49-54.

(6) Ajayan, P. M.; Ebbesen, T. W. *Rep. Prog. Phys.* **1997**, *60*, 1025-1062.

(7) Ajayan, P. M. *Chem. Rev.* **1999**, *99*, 1787-1799.

(8) Wildoer, J. W. G.; Venema, L. C.; Rinzler, A. G.; Smalley, R. E.; Dekker, C. *Nature* **1998**, *391*, 59-62.

(9) Baughman, R. H.; Zakhidov, A. A.; de Heer, W. A. *Science* **2002**, *297*, 787-792.

(10) Dujardin, E.; Ebbesen, T. W.; Krishnan, A.; Treacy, M. M. J. *Adv. Mater.* **1998**, *10*, 1472-1475.

(11) Odom, T. W.; Huang, J. L.; Kim, P.; Lieber, C. M. *Nature* **1998**, *391*, 62-64.

(12) De Heer, W. A. *Nat. Mater.* **2002**, *1*, 153-154.

(13) Li, F.; Cheng, H. M.; Bai, S.; Su, G.; Dresselhaus, M. S. *Appl. Phys. Lett.* **2000**, *77*, 3161-3163.

(14) Yu, M. F.; Files, B. S.; Arepalli, S.; Ruoff, R. S. *Phys. Rev. Lett.* **2000**, *84*, 5552-5555.

(15) Hone, J.; Batlogg, B.; Benes, Z.; Johnson, A. T.; Fischer, J. E. *Science* **2000**, *289*, 1730-1733.

(16) Wong, E. W.; Sheehan, P. E.; Lieber, C. M. *Science* **1997**, *277*, 1971-1975.

(17) Falvo, M. R.; Clary, G. J.; Taylor, R. M.; Chi, V.; Brooks, F. P.; Washburn, S.; Superfine, R. *Nature* **1997**, *389*, 582-584.

(18) Biercuk, M. J.; Llaguno, M. C.; Radosavljevic, M.; Hyun, J. K.; Johnson, A. T.; Fischer, J. E. *Appl. Phys. Lett.* **2002**, *80*, 2767-2769.

(19) Cadek, M.; Coleman, J. N.; Ryan, K. P.; Nicolosi, V.; Bister, G.; Fonseca, A.; Nagy, J. B.; Szostak, K.; Beguin, F.; Blau, W. J. *Nano. Lett.* **2004**, *4*, 353-356.

(20) Tans, S. J.; Verschueren, A. R. M.; Dekker, C. *Nature* **1998**, *393*, 49-52.

(21) Deheer, W. A.; Chatelain, A.; Ugarte, D. *Science* **1995**, *270*, 1179-1180.

(22) Rinzler, A. G.; Hafner, J. H.; Nikolaev, P.; Lou, L.; Kim, S. G.; Tomanek, D.; Nordlander, P.; Colbert, D. T.; Smalley, R. E. *Science* **1995**, *269*, 1550-1553.

(23) Kong, J.; Franklin, N. R.; Zhou, C. W.; Chapline, M. G.; Peng, S.; Cho, K. J.; Dai, H. J. *Science* **2000**, *287*, 622-625.

(24) Collins, P. G.; Bradley, K.; Ishigami, M.; Zettl, A. *Science* **2000**, *287*, 1801-1804.

(25) Hafner, J. H.; Cheung, C. L.; Lieber, C. M. *Nature* **1999**, *398*, 761-762.

(26) Dai, H. J.; Hafner, J. H.; Rinzler, A. G.; Colbert, D. T.; Smalley, R. E. *Nature* **1996**, *384*, 147-150.

(27) An, K. H.; Kim, W. S.; Park, Y. S.; Moon, J. M.; Bae, D. J.; Lim, S. C.; Lee, Y. S.; Lee, Y. H. *Adv. Funct. Mater.* **2001**, *11*, 387-392.

(28) Niu, C. M.; Sichel, E. K.; Hoch, R.; Moy, D.; Tennent, H. *Appl. Phys. Lett.* **1997**, *70*, 1480-1482.

(29) Baughman, R. H.; Cui, C. X.; Zakhidov, A. A.; Iqbal, Z.; Barisci, J. N.; Spinks, G. M.; Wallace, G. G.; Mazzoldi, A.; De Rossi, D.; Rinzler, A. G.; Jaschinski, O.; Roth, S.; Kertesz, M. *Science* **1999**, *284*, 1340-1344.

(30) Dresselhaus, M. S.; Williams, K. A.; Eklund, P. C. *MRS. Bull.* **1999**, *24*, 45-50.

(31) Tibbetts, G. G.; Meisner, G. P.; Olk, C. H. *Carbon* **2001**, *39*, 2291-2301.

(32) Zandonella, C. *Nature* **2001**, *410*, 734-735.

(33) Ye, Y.; Ahn, C. C.; Witham, C.; Fultz, B.; Liu, J.; Rinzler, A. G.; Colbert, D.; Smith, K. A.; Smalley, R. E. *Appl. Phys. Lett.* **1999**, *74*, 2307-2309.

(34) Kymakis, E.; Amaratunga, G. A. J. *Appl. Phys. Lett* **2002**, *80*, 112-114.

(35) Kymakis, E.; Alexandrou, I.; Amaratunga, G. A. J. *J. Appl. Phys.* **2003**, *93*, 1764-1768.

(36) Kymakis, E.; Amaratunga, G. A. J. *Synthetic Met.* **2004**, *142*, 161-167.

(37) Bahr, J. L.; Mickelson, E. T.; Bronikowski, M. J.; Smalley, R. E.; Tour, J. M. *Chem. Commun.* **2001**, 193-194.

(38) Chen, Y.; Haddon, R. C.; Fang, S.; Rao, A. M.; Lee, W. H.; Dickey, E. C.; Grulke, E. A.; Pendergrass, J. C.; Chavan, A.; Haley, B. E.; Smalley, R. E. *J. Mater. Res.* **1998**, *13*, 2423-2431.

(39) Hamon, M. A.; Itkis, M. E.; Niyogi, S.; Alvaraez, T.; Kuper, C.; Menon, M.; Haddon, R. C. *J. Am. Chem. Soc.* **2001**, *123*, 11292-11293.

(40) Haddon, R. C. *Science* **1993**, *261*, 1545-1550.

(41) Niyogi, S.; Hamon, M. A.; Hu, H.; Zhao, B.; Bhowmik, P.; Sen, R.; Itkis, M. E.; Haddon, R. C. *Accounts Chem. Res.* **2002**, *35*, 1105-1113.

(42) Haddon, R. C.; Scuseria, G. E.; Smalley, R. E. *Chem. Phys. Lett.* **1997**, *272*, 38-42.

(43) Liu, J.; Rinzler, A. G.; Dai, H. J.; Hafner, J. H.; Bradley, R. K.; Boul, P. J.;

Lu, A.; Iverson, T.; Shelimov, K.; Huffman, C. B.; Rodriguez-Macias, F.; Shon, Y. S.; Lee, T. R.; Colbert, D. T.; Smalley, R. E. *Science* **1998**, *280*, 1253-1256.

(44) Mawhinney, D. B.; Naumenko, V.; Kuznetsova, A.; Yates, J. T.; Liu, J.; Smalley, R. E. *Chem. Phys. Lett.* **2000**, *324*, 213-216.

(45) Hamon, M. A.; Hu, H.; Bhowmik, P.; Niyogi, S.; Zhao, B.; Itkis, M. E.; Haddon, R. C. *Chem. Phys. Lett.* **2001**, *347*, 8-12.

(46) Chen, J.; Rao, A. M.; Lyuksyutov, S.; Itkis, M. E.; Hamon, M. A.; Hu, H.; Cohn, R. W.; Eklund, P. C.; Colbert, D. T.; Smalley, R. E.; Haddon, R. C. *J. Phys. Chem. B* **2001**, *105*, 2525-2528.

(47) Kukovecz, A.; Kramberger, C.; Holzinger, M.; Kuzmany, H.; Schalko, J.; Mannsberger, M.; Hirsch, A. *J. Phys. Chem. B* **2002**, *106*, 6374-6380.

(48) Hirsch, A. *Angew. Chem. Int. Edit.* **2002**, *41*, 1853-1859.

(49) Hu, H.; Bhowmik, P.; Zhao, B.; Hamon, M. A.; Itkis, M. E.; Haddon, R. C. *Chem. Phys. Lett.* **2001**, *345*, 25-28.

(50) Banerjee, S.; Wong, S. S. *Nano. Lett.* **2002**, *2*, 195-200.

(51) Fu, K. F.; Huang, W. J.; Lin, Y.; Zhang, D. H.; Hanks, T. W.; Rao, A. M.; Sun, Y. P. *J Nanosci. Nanotechno.* **2002**, *2*, 457-461.

(52) Huang, W. J.; Taylor, S.; Fu, K. F.; Lin, Y.; Zhang, D. H.; Hanks, T. W.; Rao, A. M.; Sun, Y. P. *Nano. Lett.* **2002**, *2*, 311-314.

(53) Frehill, F.; Vos, J. G.; Benrezzak, S.; Koos, A. A.; Konya, Z.; Ruther, M. G.; Blau, W. J.; Fonseca, A.; Nagy, J. B.; Biro, L. P.; Minett, A. I.; Panhuis, M. I. H. *J. Am. Chem. Soc.* **2002**, *124*, 13694-13695.

(54) Holzinger, M.; Vostrowsky, O.; Hirsch, A.; Hennrich, F.; Kappes, M.; Weiss, R.; Jellen, F. *Angew. Chem. Int. Edit.* **2001**, *40*, 4002-4005.

(55) Chen, J.; Hamon, M. A.; Hu, H.; Chen, Y. S.; Rao, A. M.; Eklund, P. C.;

Haddon, R. C. *Science* **1998**, *282*, 95-98.

(56) Pekker, S.; Salvetat, J. P.; Jakab, E.; Bonard, J. M.; Forro, L. *J. Phys. Chem. B* **2001**, *105*, 7938-7943.

(57) Mickelson, E. T.; Chiang, I. W.; Zimmerman, J. L.; Boul, P. J.; Lozano, J.; Liu, J.; Smalley, R. E.; Hauge, R. H.; Margrave, J. L. *J. Phys. Chem. B* **1999**, *103*, 4318-4322.

(58) Mickelson, E. T.; Huffman, C. B.; Rinzler, A. G.; Smalley, R. E.; Hauge, R. H.; Margrave, J. L. *Chem. Phys. Lett.* **1998**, *296*, 188-194.

(59) Boul, P. J.; Liu, J.; Mickelson, E. T.; Huffman, C. B.; Ericson, L. M.; Chiang, I. W.; Smith, K. A.; Colbert, D. T.; Hauge, R. H.; Margrave, J. L.; Smalley, R. E. *Chem. Phys. Lett.* **1999**, *310*, 367-372.

(60) Bahr, J. L.; Yang, J. P.; Kosynkin, D. V.; Bronikowski, M. J.; Smalley, R. E.; Tour, J. M. *J. Am. Chem. Soc.* **2001**, *123*, 6536-6542.

(61) Bahr, J. L.; Tour, J. M. *Chem. Mater.* **2001**, *13*, 3823-3824.

(62) Georgakilas, V.; Kordatos, K.; Prato, M.; Guldi, D. M.; Holzinger, M.; Hirsch, A. *J. Am. Chem. Soc.* **2002**, *124*, 760-761.

(63) Coleman, K. S.; Bailey, S. R.; Fogden, S.; Green, M. L. H. *J. Am. Chem. Soc.* **2003**, *125*, 8722-8723.

(64) Umek, P.; Seo, J. W.; Hernadi, K.; Mrzel, A.; Pechy, P.; Mihailovic, D. D.; Forro, L. *Chem. Mater.* **2003**, *15*, 4751-4755.

(65) Ying, Y. M.; Saini, R. K.; Liang, F.; Sadana, A. K.; Billups, W. E. *Org. Lett.* **2003**, *5*, 1471-1473.

(66) Riggs, J. E.; Guo, Z. X.; Carroll, D. L.; Sun, Y. P. *J. Am. Chem. Soc.* **2000**, *122*, 5879-5880.

(67) Sun, Y. P.; Huang, W. J.; Lin, Y.; Fu, K. F.; Kitaygorodskiy, A.; Riddle, L. A.; Yu, Y. J.; Carroll, D. L. *Chem. Mater.* **2001**, *13*, 2864-2869.

(68) Qin, S. H.; Qin, D. Q.; Ford, W. T.; Resasco, D. E.; Herrera, J. E. *Macromolecules* **2004**, *37*, 752-757.

(69) Yao, Z. L.; Braidy, N.; Botton, G. A.; Alex, A. T. *J. Am. Chem. Soc.* **2003**, *125*, 16015-16024.

(70) Sun, Y. P.; Fu, K. F.; Lin, Y.; Huang, W. J. *Accounts Chem. Res.* **2002**, *35*, 1096-1104.

(71) Lin, Y.; Rao, A. M.; Sadanadan, B.; Kenik, E. A.; Sun, Y. P. *J. Phys. Chem. B* **2002**, *106*, 1294-1298.

(72) Huang, W. J.; Lin, Y.; Taylor, S.; Gaillard, J.; Rao, A. M.; Sun, Y. P. *Nano. Lett.* **2002**, *2*, 231-234.

(73) Hill, D. E.; Lin, Y.; Allard, L. F.; Sun, Y. P. *Int. J. Nanosci.* **2002**, *1*, 213-221.

(74) Krusic, P. J.; Wasserman, E.; Keizer, P. N.; Morton, J. R.; Preston, K. F. *Science* **1991**, *254*, 1183-1185.

(75) Morton, J. R.; Preston, K. F.; Krusic, P. J.; Hill, S. A.; Wasserman, E. *J Phys. Chem.-Us* **1992**, *96*, 3576-3578.

(76) Morton, J. R.; Negri, F.; Preston, K. F. *Accounts Chem. Res.* **1998**, *31*, 63-69.

(77) Shaffer, M. S. P.; Koziol, K. *Chem. Commun.* **2002**, 2074-2075.

(78) Szwarc, M. *Nature* **1956**, *178*, 1168-1169.

(79) Miyamoto, M.; Sawamoto, M.; Higashimura, T. *Macromolecules* **1984**, *17*, 265-268.

(80) Veregin, R. P. N.; Georges, M. K.; Hamer, G. K.; Kazmaier, P. M. *Macromolecules* **1995**, *28*, 4391-4398.

(81) Hawker, C. J.; Barclay, G. G.; Orellana, A.; Dao, J.; Devonport, W. *Macromolecules* **1996**, *29*, 5245-5254.

(82) Hawker, C. J.; Barclay, G. G.; Dao, J. L. *J. Am. Chem. Soc.* **1996**, *118*, 11467-11471.

(83) Hawker, C. J.; Bosman, A. W.; Harth, E. *Chem. Rev.* **2001**, *101*, 3661-3688.

(84) Matyjaszewski, K.; Patten, T. E.; Xia, J. H. *J. Am. Chem. Soc.* **1997**, *119*, 674-680.

(85) Matyjaszewski, K.; Coca, S.; Gaynor, S. G.; Wei, M. L.; Woodworth, B. E. *Macromolecules* **1997**, *30*, 7348-7350.

(86) Matyjaszewski, K.; Xia, J. H. *Chem. Rev.* **2001**, *101*, 2921-2990.

(87) Kamigaito, M.; Ando, T.; Sawamoto, M. *Chem. Rev.* **2001**, *101*, 3689-3745.

(88) Chiefari, J.; Chong, Y. K.; Ercole, F.; Krstina, J.; Jeffery, J.; Le, T. P. T.; Mayadunne, R. T. A.; Meijs, G. F.; Moad, C. L.; Moad, G.; Rizzardo, E.; Thang, S. H. *Macromolecules* **1998**, *31*, 5559-5562.

(89) Chong, Y. K.; Le, T. P. T.; Moad, G.; Rizzardo, E.; Thang, S. H. *Macromolecules* **1999**, *32*, 2071-2074.

(90) Mayadunne, R. T. A.; Rizzardo, E.; Chiefari, J.; Chong, Y. K.; Moad, G.; Thang, S. H. *Macromolecules* **1999**, *32*, 6977-6980.

(91) Moad, G.; Chiefari, J.; Chong, Y. K.; Krstina, J.; Mayadunne, R. T. A.; Postma, A.; Rizzardo, E.; Thang, S. H. *Polym. Int.* **2000**, *49*, 993-1001.

(92) Georges, M. K.; Veregin, R. P. N.; Kazmaier, P. M.; Hamer, G. K.; Saban, M. *Macromolecules* **1994**, *27*, 7228-7229.

(93) Malmstrom, E.; Miller, R. D.; Hawker, C. J. *Tetrahedron* **1997**, *53*, 15225-15236.

(94) Benoit, D.; Chaplinski, V.; Braslau, R.; Hawker, C. J. *J. Am. Chem. Soc.* **1999**, *121*, 3904-3920.

(95) Nikolaev, P.; Bronikowski, M. J.; Bradley, R. K.; Rohmund, F.; Colbert, D. T.; Smith, K. A.; Smalley, R. E. *Chem. Phys. Lett.* **1999**, *313*, 91-97.